

Electronic Supporting Information

Utilizing formation of dye aggregates with aggregation-induced emission characteristics for enhancement of two-photon absorption

Adrian Justyniarski,^a Jan K. Zaręba,^a Piotr Hańczyc,^b Piotr Fita,^c Marta Chołuj,^d
Robert Zaleśny,^d Marek Samoć,^{*,a}

^a Advanced Materials Engineering and Modelling Group, Faculty of Chemistry, Wrocław University of Science and Technology, Wyb. Wyspiańskiego 27, 50-370, Wrocław, Poland

^b Institute of Physical Chemistry, Polish Academy of Sciences, Kasprzaka 44/52, 01-224 Warsaw, Poland

^c Institute of Experimental Physics, Faculty of Physics, University of Warsaw, Pasteura 5, 02-093 Warsaw, Poland

^d Department of Physical and Theoretical Chemistry, Faculty of Chemistry, Wrocław University of Science and Technology, Wyb. Wyspiańskiego 27, 50-370, Wrocław, Poland

* email: marek.samoc@pwr.edu.pl

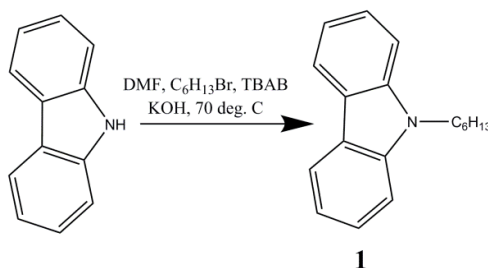
Techniques and instrumentation

^1H , $^{13}\text{C}\{^1\text{H}\}$, $^{31}\text{P}\{^1\text{H}\}$ NMR spectra were recorded either on a Jeol JNM-ECZ 400S Research FT NMR spectrometer (JEOL Ltd., Tokyo, Japan) operating at 400 MHz (for ^1H), or with the use of a Bruker Avance 600 spectrometer operating at 600 MHz (for ^1H). Mid-infrared (MIR) and far-infrared (FIR) spectra were obtained on a VERTEX 70V FT-IR spectrometer (Bruker Optik GmbH, Ettlingen, Germany) in attenuated total reflection (ATR) measurement mode at room temperature. Absorption spectra in the UV-Vis region were acquired in 1 cm quartz cuvettes using a Jasco V-670 spectrophotometer.

Synthetic procedures

Starting materials were of reagent grade purity and were obtained from commercial sources and used without further purification. Dioxane and DMF were kept over 3Å Aldrich molecular sieves.

Synthesis of *N*-hexylcarbazole (1):



In two-neck flask were placed carbazole (5.00 g, 0.0299 mol), 1-bromohexane (5.52 cm^3 , 0.0389 mol), KOH (2.18 g, 0.0389 mol), TBAB (tetrabutylammonium bromide, 0.967 g, 0.00299 mol), and DMF (50 cm^3). Obtained mixture was stirred at 70°C for 24 hours. After cooling down, water and chloroform were added (each 100 cm^3) and thoroughly shaken. Organic layer was separated, and inorganic layer was extracted again with chloroform (100 cm^3). Combined organic extracts were washed with water (100 cm^3), two times with NaCl saturated solution ($2 \times 100\text{ cm}^3$) and finally dried with anhydrous Na_2SO_4 . Yellowish oil was subjected to column chromatography on silica gel, using hexane as a mobile phase. Colorless oil, yield 7.51 g, 84 %.

^1H NMR (600 MHz, CDCl_3 , 300K) δ 8.12 (d, $J = 7.7\text{ Hz}$, 2H), 7.48 (t, $J = 7.6\text{ Hz}$, 2H), 7.42 (d, $J = 8.1\text{ Hz}$, 2H), 7.24 (t, $J = 7.4\text{ Hz}$, 2H), 4.31 (t, $J = 7.3\text{ Hz}$, 2H), 1.88 (dt, $J = 15.0, 7.5\text{ Hz}$, 2H), 1.44-1.35 (m, 2H), 1.35-1.22 (m, 4H), 0.88 (t, $J = 7.0\text{ Hz}$, 3H).

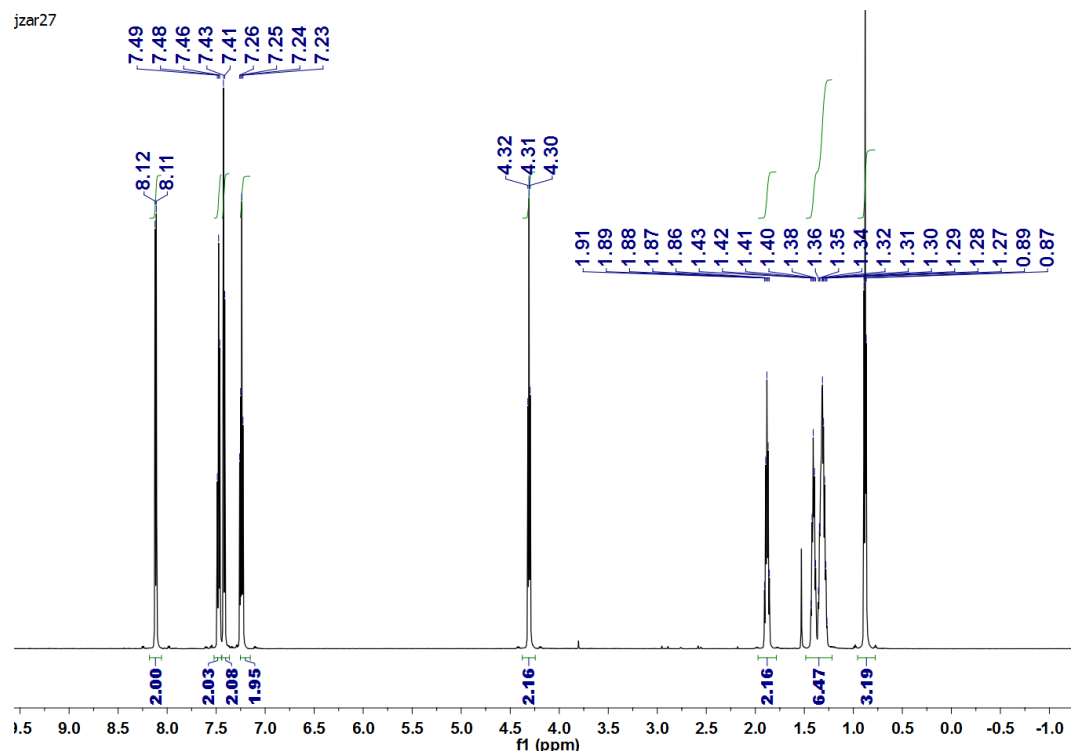
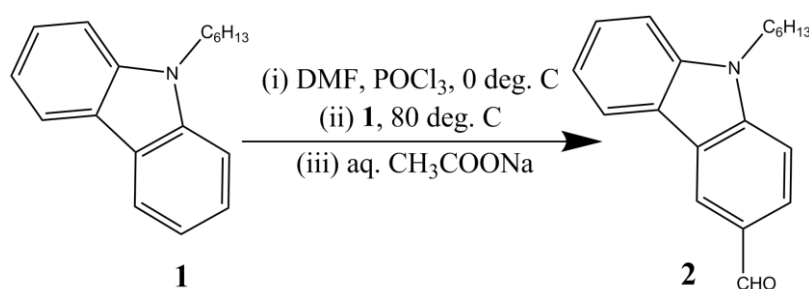


Fig. S1. ^1H NMR (600 MHz, CDCl_3) spectrum of *N*-hexylcarbazole (1)

Synthesis of 3-formyl-9-(*N*-hexyl)carbazole (2):



In two-neck flask was placed DMF (1.133 g, 0.0155 mol). Next, POCl_3 (2.30 g, 15.00 mmol) under the atmosphere of nitrogen was added in small portion at 0 deg. C. The mixture was stirred till the glassy solid was obtained. It was heated to 80 deg. C and *N*-hexylcarbazole (1) was added in one portion (3.00 g, 0.0119 mmol). Initially, dark green coloration is observed, which with time turns to dark brown (heating 4 hours, under nitrogen).

After cooling, the mixture was transferred to the large excess of 10% aqueous solution of sodium acetate. Obtained brown solid was filtered out, washed with water and dried in air. Crude product was subjected to column chromatography on silica gel, using chloroform / hexane = 1:1 (v/v) as a mobile phase. Yellowish oil, crystallizing after some time, was obtained. Yield: 2.69 g, 81 %.

^1H NMR (600 MHz, CDCl_3) δ 9.85 (s, 1H), 8.30 (s, 1H), 7.88 (d, J = 7.8 Hz, 1H), 7.75 (d, J = 8.5 Hz, 1H), 7.32 (m, 1H), 7.19 (d, J = 8.2 Hz, 1H), 7.15 (d, J = 8.5 Hz, 1H), 7.10 (m, 1H), 3.97 (t, J = 7.2 Hz, 2H), 1.68–1.47 (m, 2H), 1.20–0.95 (m, 6H), 0.68 (t, J = 5.9 Hz, 3H).

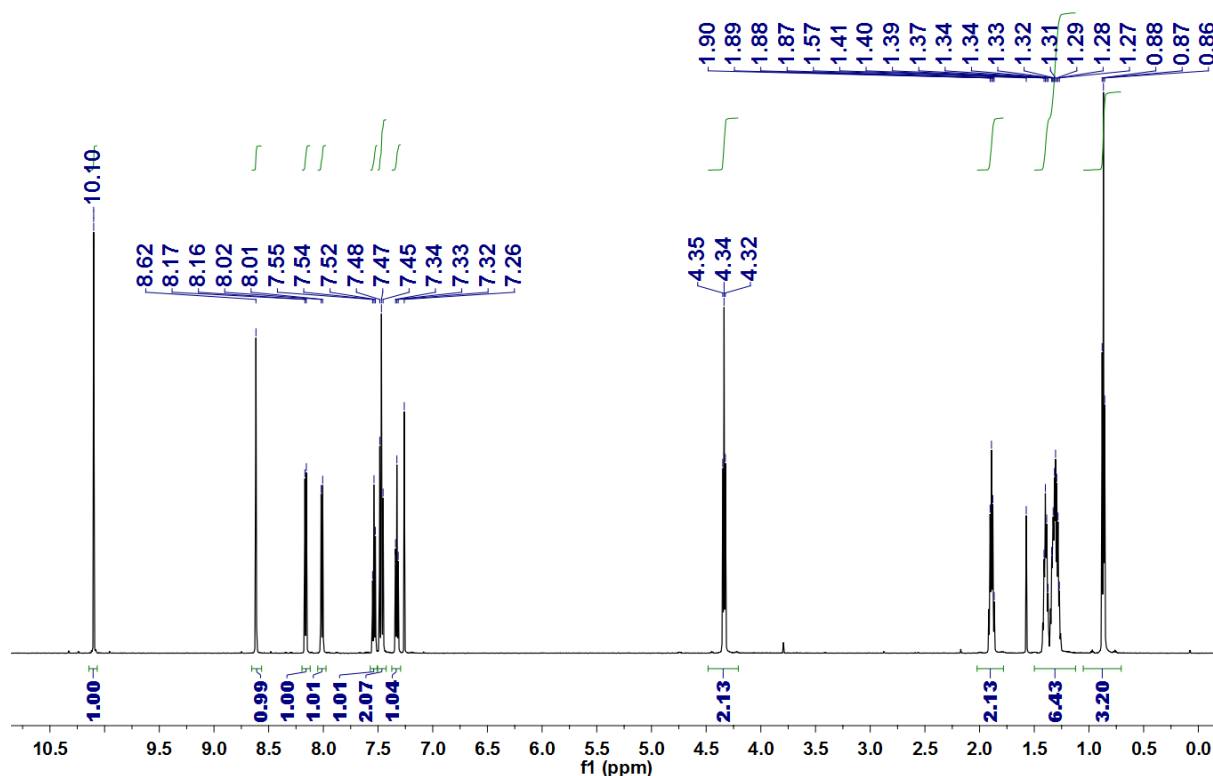
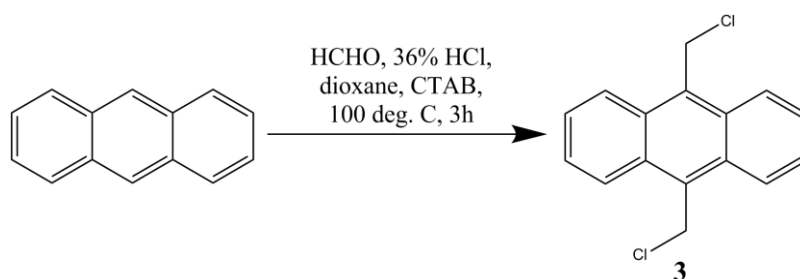


Fig. S2. ^1H NMR (600 MHz, CDCl_3) spectrum of 3-formyl-9-(*N*-hexyl)carbazole (2)

Synthesis of 9,10-bis(chloromethyl)anthracene (3):



In two-neck flask were placed anthracene (9.79 g, 0.055 mol), paraformaldehyde (3.795 g, 0.1265 mol), CTAB (cetyltrimethylammonium bromide, 2.00 g, 0.0055 mol), dioxane (100 cm^3), and 36% HCl (100 cm^3). The obtained heterogenous mixture was heated at 100 deg. C for 3 hours. During heating 36% HCl (50 cm^3) was slowly dropped to the mixture, in order to maintain high concentration of HCl in the reaction system. After cooling down, the fluffy yellow precipitate was gravity filtered, washed with large amount of water and dried in air. Crude product has been crystallized from toluene twice, giving light yellow small needles as the product. Yield: 7.41 g, 49 %.

^1H NMR (400 MHz, $\text{DMSO}-d_6$) δ 8.50-8.53 (m, 4H), 7.71-7.73 (m, 4H), 5.87(s, 4H).

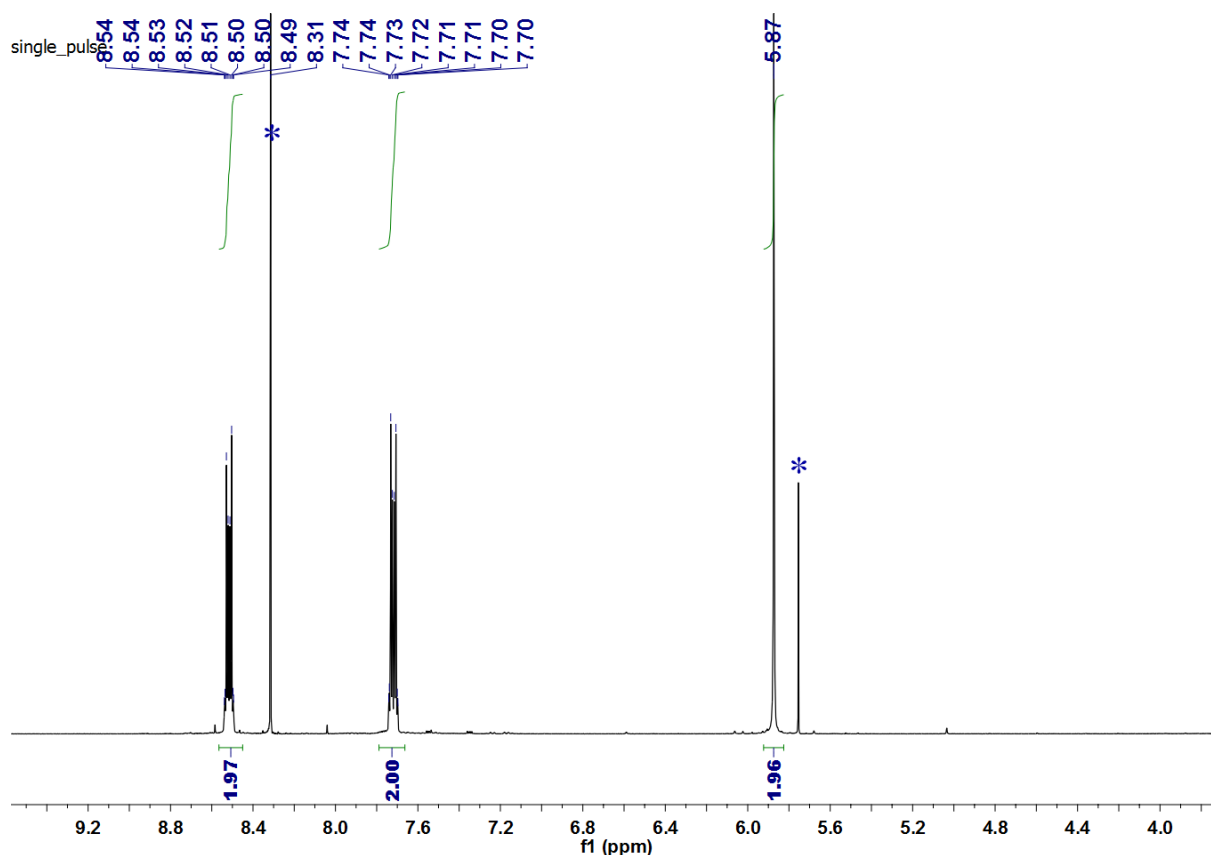
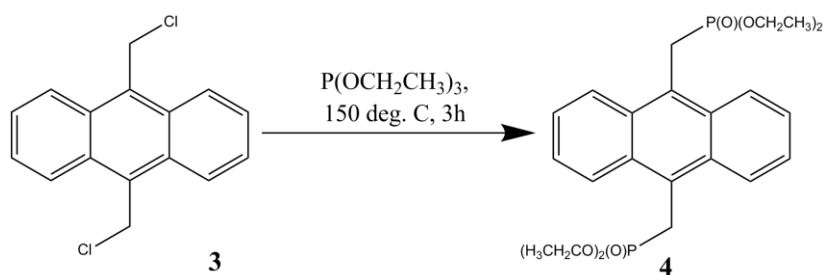


Fig. S3. ^1H NMR (400 MHz, DMSO-d_6) of 9,10-bis(chloromethyl)anthracene (**3**)

Synthesis of 9,10-bis(dietoxyphosphorylmethyl)anthracene (**4**):



In a two-neck flask were placed 9,10-bis(chloromethyl)anthracene (2.50 g, 0.0091 mol), and triethyl phosphite (6 cm³, 0.0350 mol). The mixture was heated to 150 deg. C under constant flow of nitrogen in order to remove ethyl chloride (which is necessary for high yield of reaction, since ethyl chloride, can consume triethyl phosphite in consecutive Arbuzov reaction). After four hours the volatiles were distilled off under reduced pressure at the same temperature. Orange-colored crude product was crystallized from the ethyl acetate / cyclohexane mixture. Light yellow crystals, 2.837 g. Another crop

of compound is obtained from column chromatography of supernatant from crystallization (silica-gel, eluent: chloroform / methanol = 10:1 (v/v)), 0.822 g. Total yield: 3.659 g, 84 %.

^1H NMR (400 MHz, CDCl_3) δ 8.38-8.36 (m, 4H), 7.58-7.55 (m, 4H), 4.23 (d, 4H, $J_{\text{H-P}} = 19.8$ Hz), 3.91- 3.86 (m, 4H), 3.82-3.78(m, 4H), 1.06 (t, 12H, $J = 7.2$ Hz).

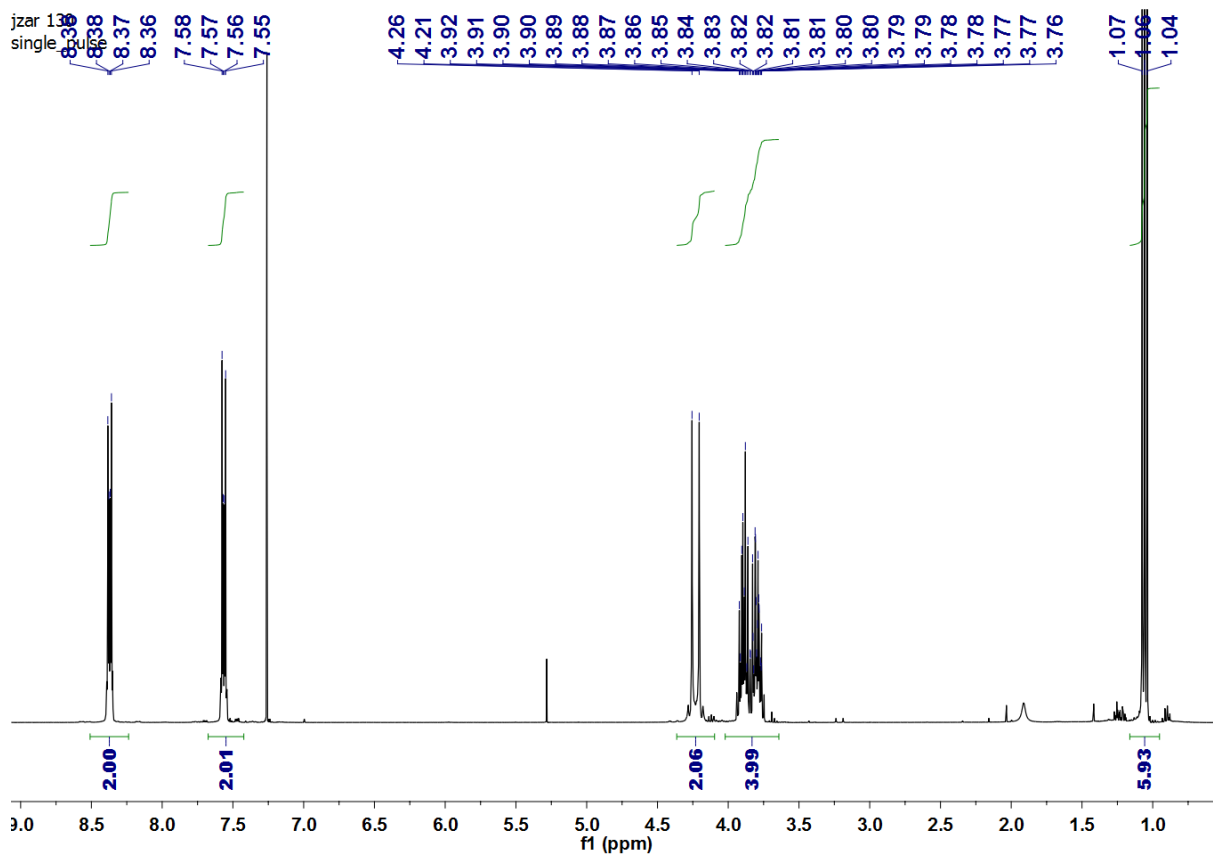
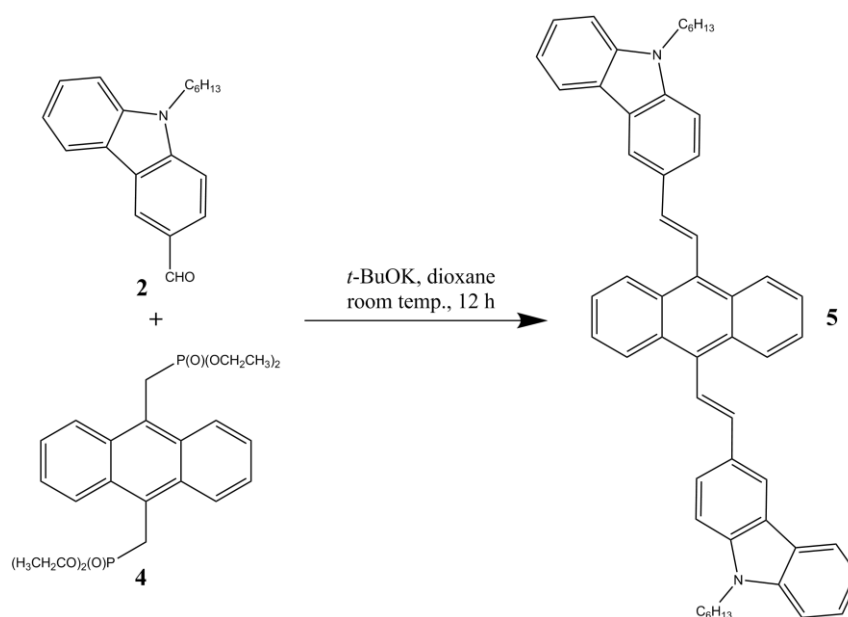


Fig. S4. ^1H NMR (400 MHz, CDCl_3) spectrum of 9,10-bis(diethoxyphosphorylmethyl)anthracene (4)

Synthesis of 9,10-bis(*N*-hexylcarbazol-3-yl-vinyl-2)anthracene (5):



In the flask was placed 9,10-bis(dietoxyphosphorylmethyl)anthracene (1.000 g, 0.0021 mol), 3-formyl-9-(*N*-hexyl)carbazole (1.518 g, 0.0054 mol), and dioxane (60 cm³). After dissolution of those reagents potassium tertbutanolate was added (0.90 g, 0.008 mol). Reaction was stirred at room temperature for 12 hours. After that time an excess of water was added (approx. 200 cm³). The orange precipitate was filtered out and dried. Crude product was extracted three times with boiling methanol (3 x 50 cm³). Light-orange methanolic extracts were discarded; the remaining yellow solid was subjected to column chromatography on silica gel two times, using chloroform / hexane = 4:1 (v/v) as an eluent. Yellow solid, yield: 0.902 g, 59 %.

¹H NMR (600 MHz, CDCl₃) δ 8.60 – 8.48 (m, 4H), 8.40 (d, *J* = 1.2 Hz, 2H), 8.18 (d, *J* = 7.7 Hz, 2H), 7.99 (d, *J* = 16.4 Hz, 2H), 7.88 (dd, *J* = 8.4, 1.5 Hz, 2H), 7.55 – 7.47 (m, 8H), 7.45 (d, *J* = 8.2 Hz, 2H), 7.28 (t, *J* = 7.3 Hz, 2H), 7.16 (d, *J* = 16.4 Hz, 2H), 4.36 (t, *J* = 7.2 Hz, 4H), 2.01 – 1.88 (m, 4H), 1.50 – 1.39 (m, 4H), 1.39 – 1.19 (m, 8H), 0.90 (t, *J* = 7.1 Hz, 6H).

¹³C NMR (151 MHz, CDCl₃) δ 140.97, 140.47, 138.27, 133.07, 129.83, 128.64, 126.73, 125.89, 125.10, 124.45, 123.33, 122.97, 122.33, 120.57, 119.08, 118.78, 109.01, 108.94, 43.29, 31.65, 29.04, 27.03, 22.60, 14.07.

MS (ESI) *m/z* (M⁺) calc. 728.4130, found 728.4098.

NMR spectra of BHCVA

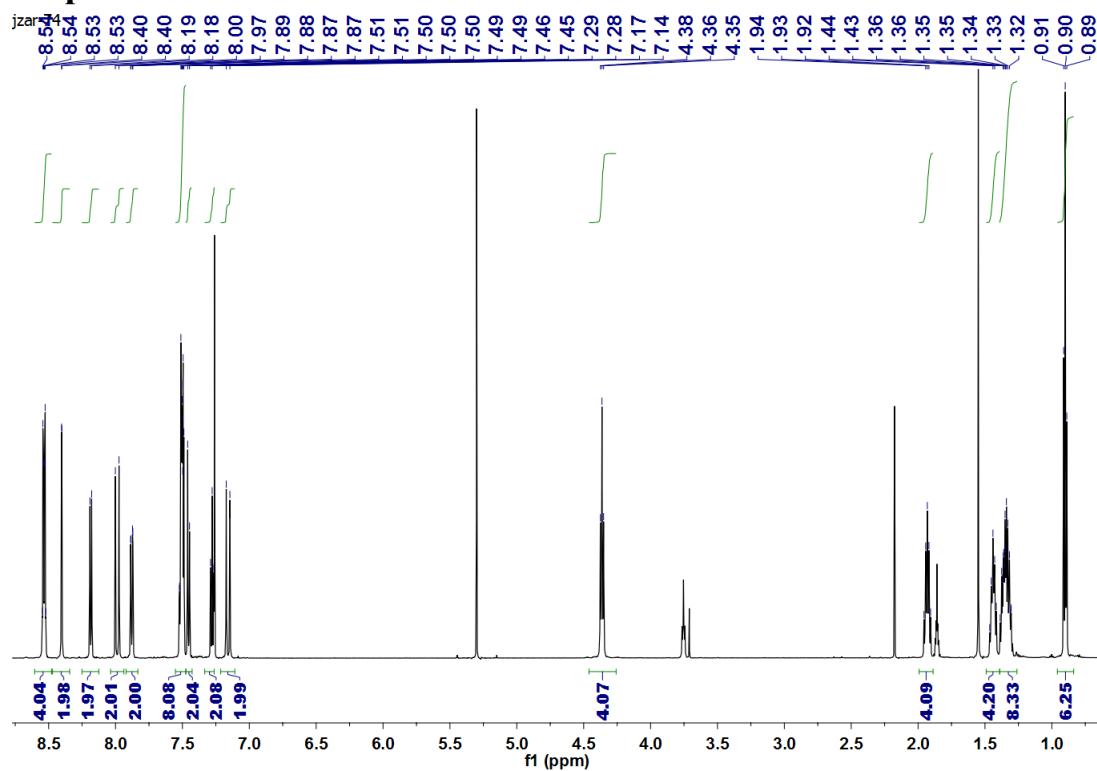


Fig. S5. BHCVA ¹H NMR spectrum

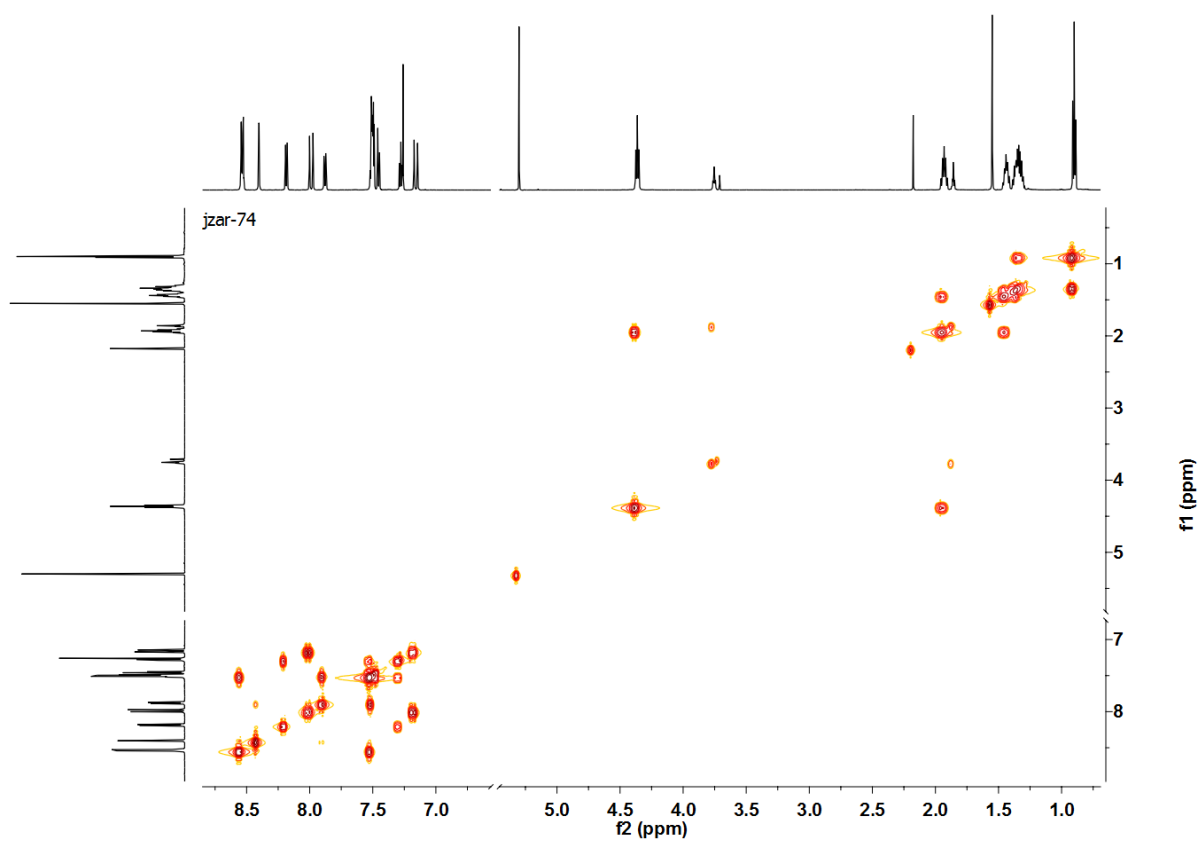


Fig. S6. BHCVA ¹H-¹H COSY correlation spectrum

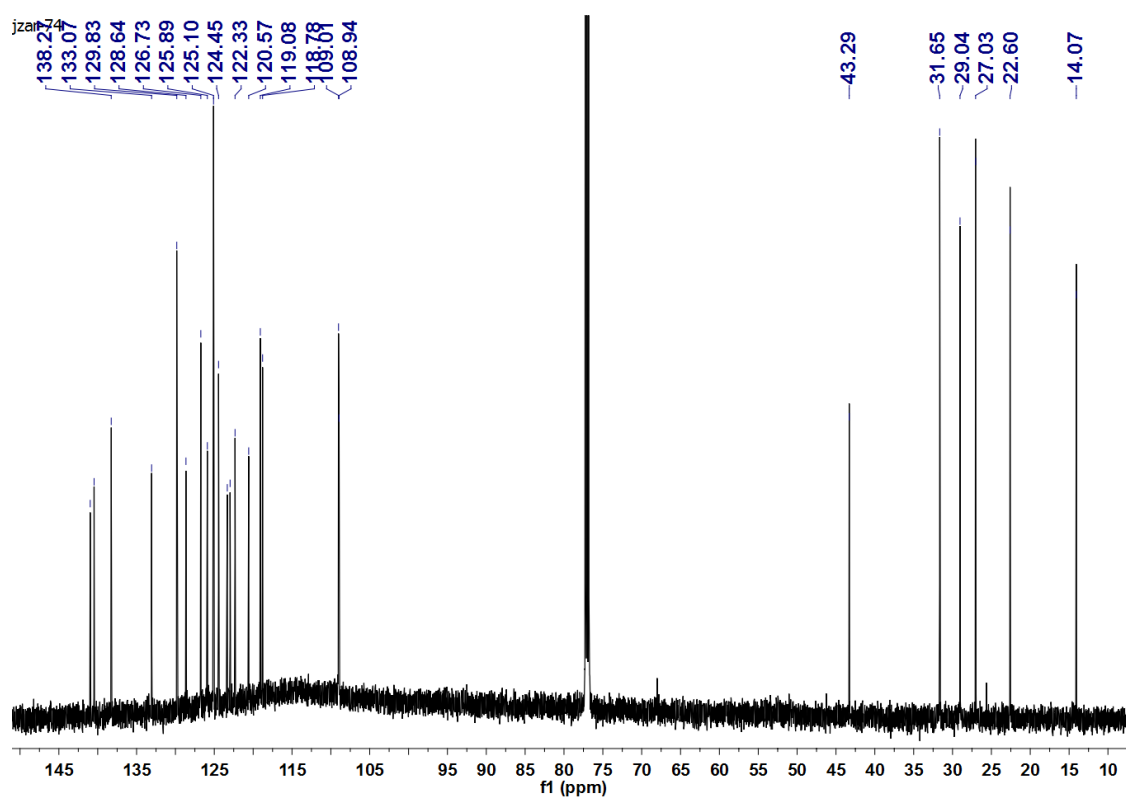


Fig. S7. BHCVA ¹³C NMR spectrum

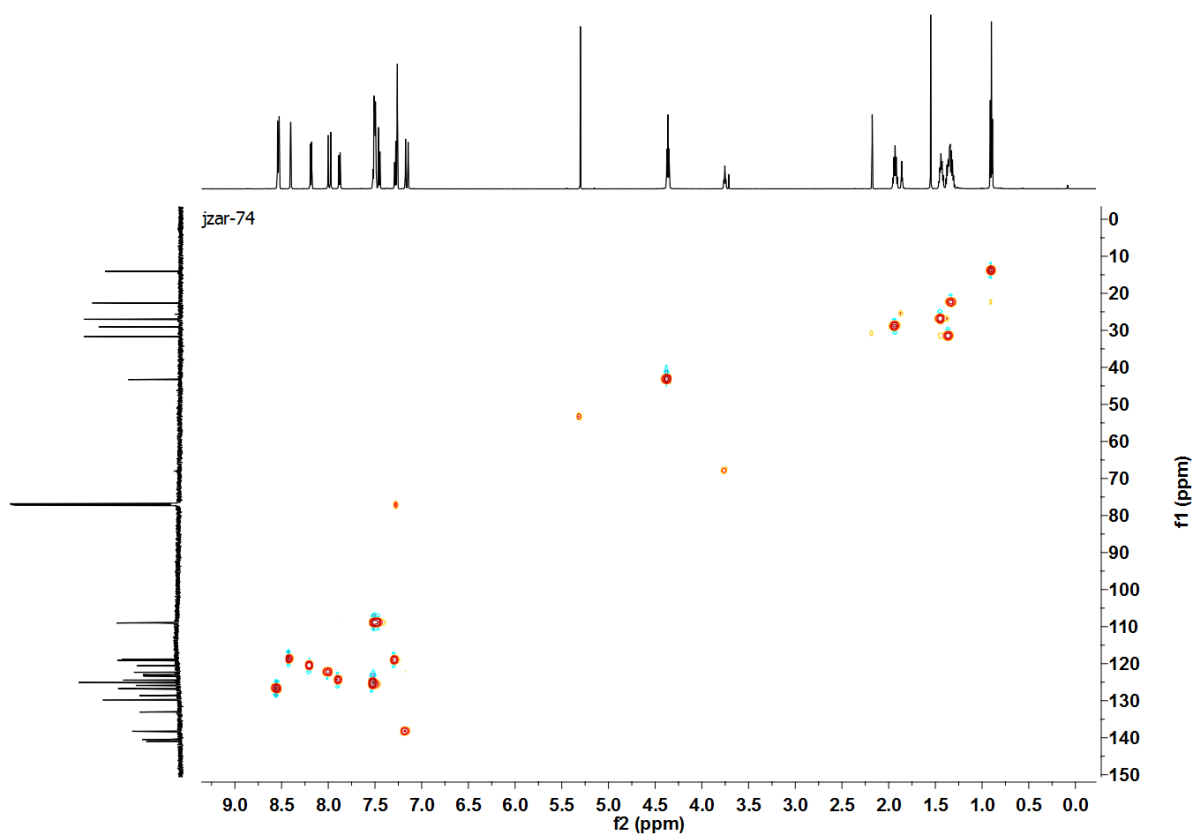


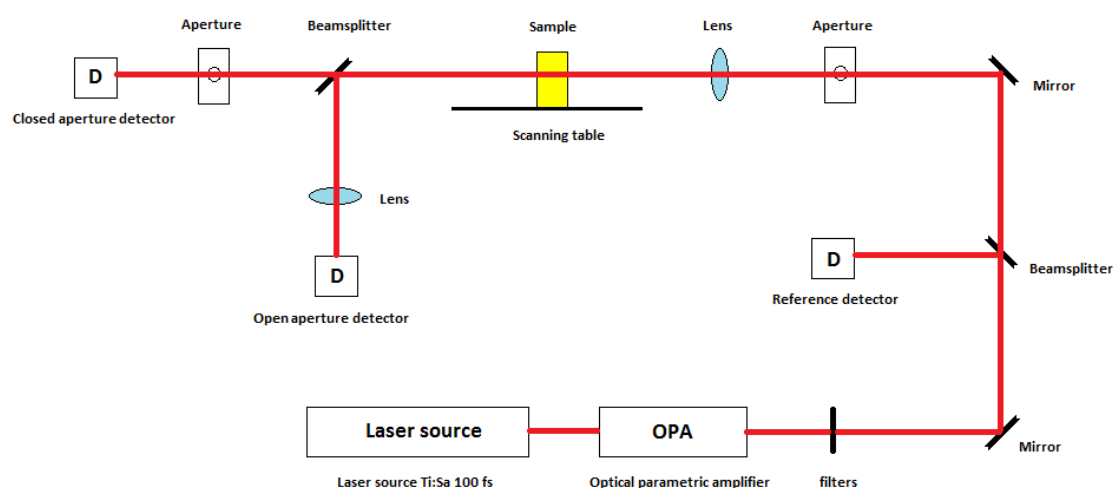
Fig. S8. BHCVA ¹H-¹³C HSQC correlation spectrum

Z-scan experiment details

The Z-scan technique is used to measure nonlinear refractive index (n_2) and nonlinear absorption coefficient (β). Both quantities can be measured simultaneously by monitoring changes in laser power of a focused laser beam on open aperture (OA) and closed aperture (CA) detectors placed in the far field, as the sample travels in the z direction.

The Z-scan measurements were performed as previously described, with some modifications¹. In order to exclude the contributions of solvent and cuvette cell to the values of NLO parameters, we have used a calculation method, in which the real and imaginary parts of the cubic hyperpolarizability, γ , or the corresponding two-photon cross sections, (σ_2), are derived from the difference between the Z-scan traces obtained for the cell filled with solvent(s) and the cell with the solution (of the same solvent composition) of **BHCVA** aggregates.

Z-scan studies were performed using a femtosecond laser system comprising a Quantronix Integra-C regenerative amplifier operating as an 800 nm pump and a Quantronix-Palitra-FS optical parametric amplifier. The latter was used to deliver wavelength tunable pulses (available range from 500 up to 2000 nm) with the duration <130 fs, and a repetition rate of 1 kHz. For investigations of **BHCVA** aggregates we used the range of 625 – 1350 nm. The Z-scan setup is presented in Scheme S1.



Scheme S1. Setup for Z-scan experiment

Aggregate samples for NLO studies were prepared in exactly the same way as for one-photon experiments, however, samples in which microcrystal precipitation of **BHCVA** occurred were not investigated (due to excessive scattering). The concentration for each solution was set to 2.74 mM which allowed to have sufficiently strong signals in the Z-scan measurements as well as allowed to obtain stable solutions of aggregates in THF-acetone and chloroform-acetone solvent systems.

Experimental open aperture (OA) and closed aperture (CA) traces were fitted using theoretical expressions derived by Sheikh-Bahae et al.²

Fluorescence lifetime

The nanosecond fluorescence kinetics was investigated with the use of Time-Correlated Single-Photon Counting (TCSPC) method. For TCSPC measurements we used a Becker&Hickl system constructed from a TCSPC Module (SPC-130-EM) and a hybrid PMT detector (HPM-100-06) with detector control card (DCC 100) mounted to a Princeton Instruments spectrograph (Acton SpectraPro-2300i).

The sample was excited with a 375 nm picosecond laser diode (BDL-375-SMC) in the 20MHz repetition mode (which corresponds to 50 ns collection time window). The fluorescence lifetime values were calculated, after elimination of the instrument response function (IRF) contribution, which accounted for ~200 ps.

Excited state dynamics

The femtosecond pump-probe setup is based on a Legend Elite Duo (Coherent, Inc.) Ti:sapphire regenerative amplifier delivering 800 nm pulses at a repetition rate of 5 kHz, the output of which is divided and routed into two independent Noncollinear Optical Parametric Amplifiers (NOPA, TOPAS-White, Light Conversion) yielding 20–30 μ J pulses tunable from 500 to 750 nm. Outputs from the NOPAs are attenuated, to approximately 800 nJ in the case of the pump beam, and to 60 nJ in the case of the probe. A mechanical chopper, synchronized with the amplifier, blocks every second pump pulse, allowing fast switching between pumping and non-pumping regimes. The probe beam traverses a delay line consisting of a corner-cube retroreflector mounted on a motorized linear stage which can provide up to 2 ns delay between pump and probe pulses. An achromatic half-wave plate mounted after the last routing mirror is used to rotate the polarization of the probe beam to 45° with respect to the pump. A polarizing beam splitting cube separates the probe beam after the sample into two polarization components, parallel and perpendicular to the polarization of the excitation. Both components are recorded by two photodiodes so that the magic angle signal (independent of rotational diffusion of molecules in the sample) can be subsequently calculated.

The pump NOPA output was tuned to 680 nm, either to excite the sample directly in a two-photon process or, when using a frequency doubling BBO crystal in the pump beam path, to provide one-photon excitation at 340 nm. This wavelength was selected to match the lowest-energy absorption peak in the samples. The probe pulses were in both cases centered at 580 nm (the setup does not allow broad-band probing, so only kinetics at selected wavelengths can be recorded). Samples were placed in quartz cells with optical path length of 2 mm. Temporal resolution of the setup was better than 100 fs for excitation at 680 nm and degraded to approx. 200 fs with frequency-doubled excitation pulses. In any case the temporal resolution was much shorter than timescale of processes seen in the samples: in the range of tens of picoseconds for the initial rise of the signal and of the order of 100 ps for its decay. For this reason the data were analyzed simply by fitting with exponential functions because any deconvolution procedures were not needed with so well separated timescales of the instrumental response and studied processes. system that has larger density of excited-states. Stabilization of the relative orientation between donor and acceptor moieties can substantially shorten the non-radiative relaxation.

Fluorescence decay and excited state dynamics for aggregates

Fluorescence decay show significant influence of aggregation degree on excited states. Typically, the emission lifetime increases upon aggregation of AIE compounds.⁹ Indeed, fluorescence lifetime in the presence of acetone (non-solvent) becomes longer (0.58 ns and 0.71 ns for 10% and 20% acetone respectively) than in pure chloroform (0.26 ns) and THF (0.45 ns). This phenomenon is well-explained by the restriction of molecular motion, due to formation of more dense, structurally confined structures, therefore limiting non-radiative relaxation pathways. Similar behavior is observed for AIE compounds in systems with gradually changed viscosity of solution.

With the use of pump-probe experiments we have found that the increase of aggregation degree (by addition of acetone) affects significantly the excited state dynamics of BHCVA. In the presence of two

different THF/acetone volume ratios (Fig. S9b) the absorption decay times were equal to 106 ps and 88 ps, about twice shorter than in pure solvents: 267 ps in chloroform and 205 ps in THF. These results were concentration independent suggesting internal processes occurring in the chromophore. Possible explanation could be the steric hindrance of the chromophores in the aggregate that may affect the charge and energy transfers in the confined molecular that has larger density of excited states.

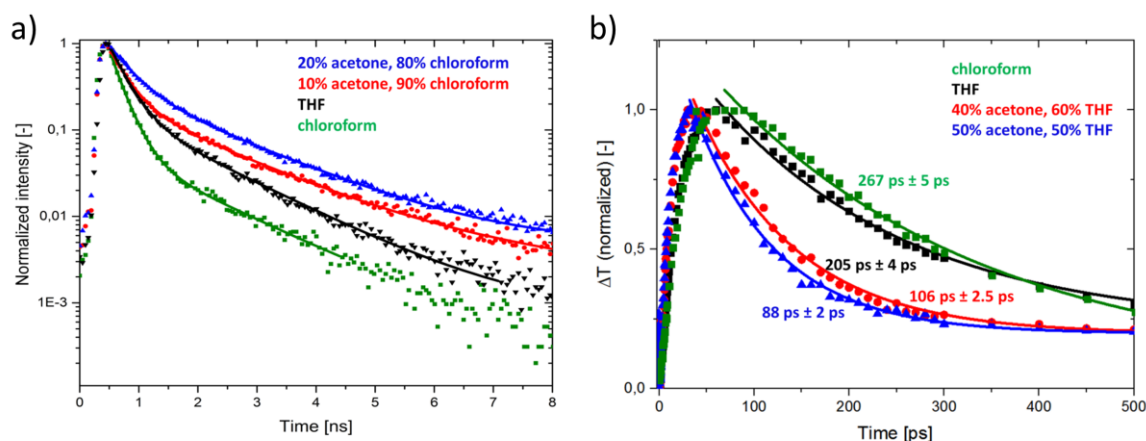


Fig. S9. (a) Fluorescence decays of BHCVA (ex. 377 nm em. 560 nm) in pure chloroform, mixtures of chloroform and acetone (10% and 20% v/v) and pure THF (b) TA dynamics monitored at 580 nm (excitation 340 nm and 680 nm) for pure chloroform, pure THF, and mixtures of THF and acetone.

Mechanochromism and thermochromism study

The influence of structural changes of BHCVA on its fluorescence was investigated in solid state. It was shown by Bu et al.³ that analogous compounds exhibit mechanochromism (methyl, propyl, pentyl, and dodecyl). Here we took a closer look at mechanochromic property of a derivative with a hexyl chain substituted at *N*-position of carbazole. The mechanochromic property of **BHCVA** was investigated through grinding a dose of pristine powder with a pestle in a mortar for several minutes. Pristine compound emits at 538 nm, with a long tail at the red side of spectrum. After grinding the emission spectrum shifts to a maximum at 598 nm, which is an effect of disturbance of a crystalline phase and formation of amorphous phase. Mechanochromism can be treated as a common property of 9,10-divinyl substituted derivatives of anthracene.⁴

Mechanochromism is often assisted by so-called vapochromism, i.e. the change of the optical properties upon exposure to certain vapors. To test response of **BHCVA** to organic vapors, a ground sample of BHCVA was introduced into a desiccator with atmosphere of dichloromethane. The sample was excited with a UV lamp (365 nm) after 5 min and 3 h of exposure to vapors (Fig.S10)

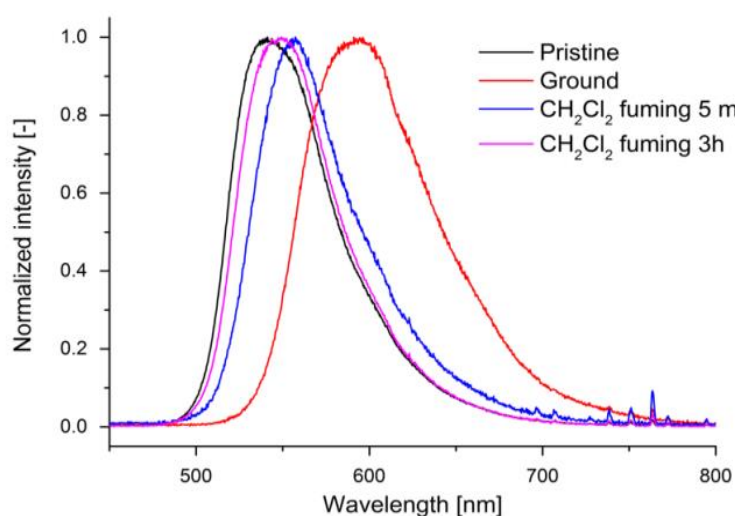


Fig. S10. UV-Vis emission spectra of BHCVA before and after grinding (black and red line, respectively). Exposure to fumes of ground BHCVA was performed with dichloromethane for 5 min and 3 h (blue and pink line, respectively).

Under such conditions an immediate response is observed: the fluorescence maximum shifts by 40 nm to the value of 558 nm. Further exposure for a total of 3 h results in a shift of 46 nm from the starting point to the value of 552 nm.

To complete mechanochromic study we have performed FT-IR studies on crystalline and ground materials (Fig. S11). Broadening and change of the relative intensity of signals suggests disruption of crystal packing (amorphization) upon grinding. Especially affected seem to be the signals corresponding to the rocking vibrations of the methylene fragments of the hexyl chains ($\sim 720\text{ cm}^{-1}$)

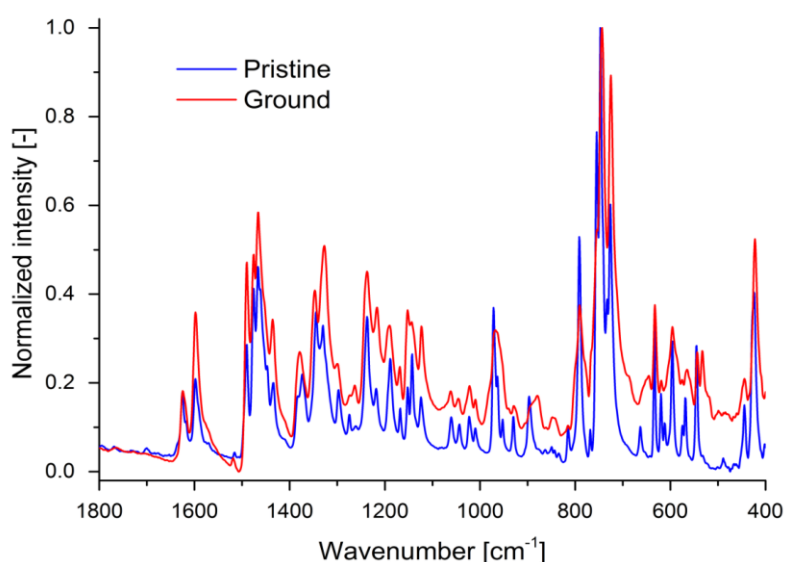


Fig. S11. A comparison of mid-IR spectra (ATR method) for pristine and ground BHCVA.

We have also investigated response of fluorescence of bulk **BHCVA** to temperature changes (thermochromism) as shown in Fig. S12 and S13. Pristine powder of **BHCVA** was deposited on a heating plate covered with glass substrate to prevent rapid temperature decay. Temperature of the

plate was changed from 23 °C to 180 °C (with 4 ± 1 °C step), controlled with thermocouple. The stabilization time was 2 minutes. The spectrum was measured on illumination of the powder with a UV lamp (365 nm). Emitted radiation was collected using an Ocean Optics spectrometer, collection time 1000 ms, averaged 5 times. Spectral red shift of the maximum in the temperature range between 25°C and 150°C is approximately linear (Fig. S13). It is reasonable to assume that temperature influences orientation of molecules and results in continuous transition from crystalline toward disordered, amorphous phase. Further increase of temperature above 150°C results in rapid decrease in fluorescence intensity, deviation from linear trend in emission shift and visible decomposition of material.

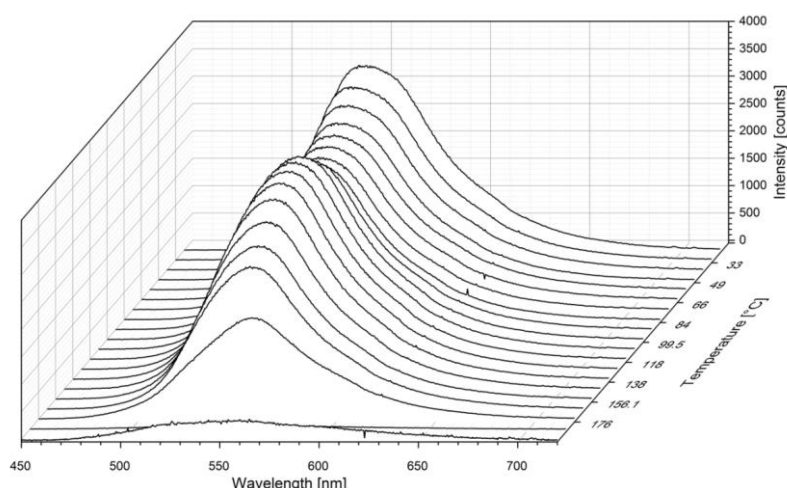


Fig. S12. Emission spectra of BHCVA collected during thermochromic experiment.

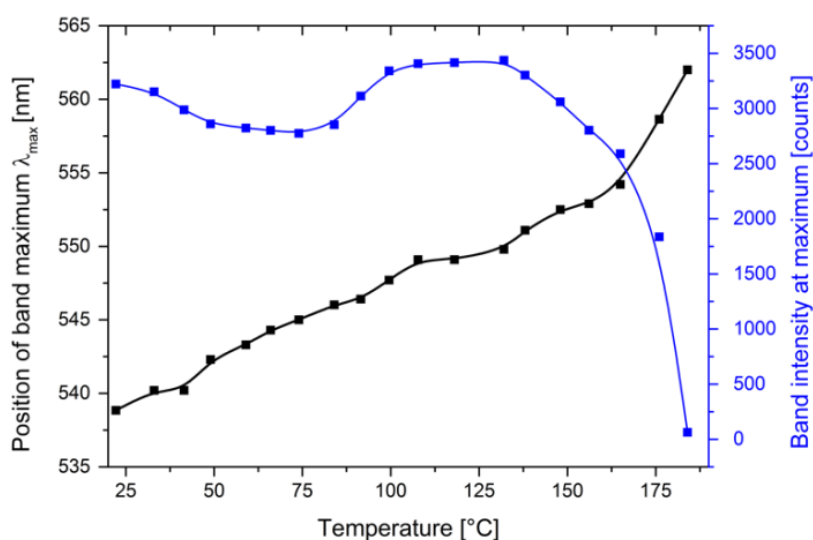


Fig. S13. Change of fluorescence maximum for BHCVA powder against temperature. The black dots represent position of intensity maximum and blue dots represent value of maximum intensity. Excitation was performed with 365 nm. Lines are used to guide eyes.

Confirmation of the AIE property

AIE nature of **BHCVA** was confirmed through gradual addition of water as non-solvent to solution of **BHCVA** in THF. Final concentration of **BHCVA** is 5 μM in each probe, with assumption that volume contraction is neglected. For low water content in solution **BHCVA** exhibits only weak fluorescence. After reaching a point when the water content comprises 50% in solution, **BHCVA** starts to bulk precipitate out of solution with fluorescence maximum at 529 nm, the same as freshly crystallized **BHCVA**. Further increase of water fraction above 70% results in formation of highly dispersive aggregates whose fluorescence maximum is shifted to 561 nm and increased in intensity (Fig. S14).

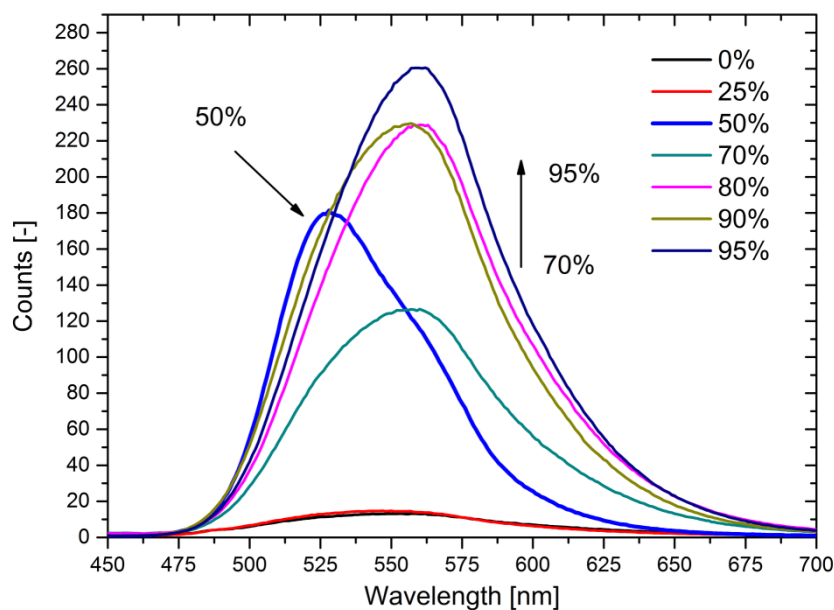


Fig. S14. Fluorescence of BHCVA in diluted THF solution (black line) subsequently titrated with water. In all samples the final molar concentration is 5 μM .

Open aperture Z-scan traces in the three-photon region and degradation experiment

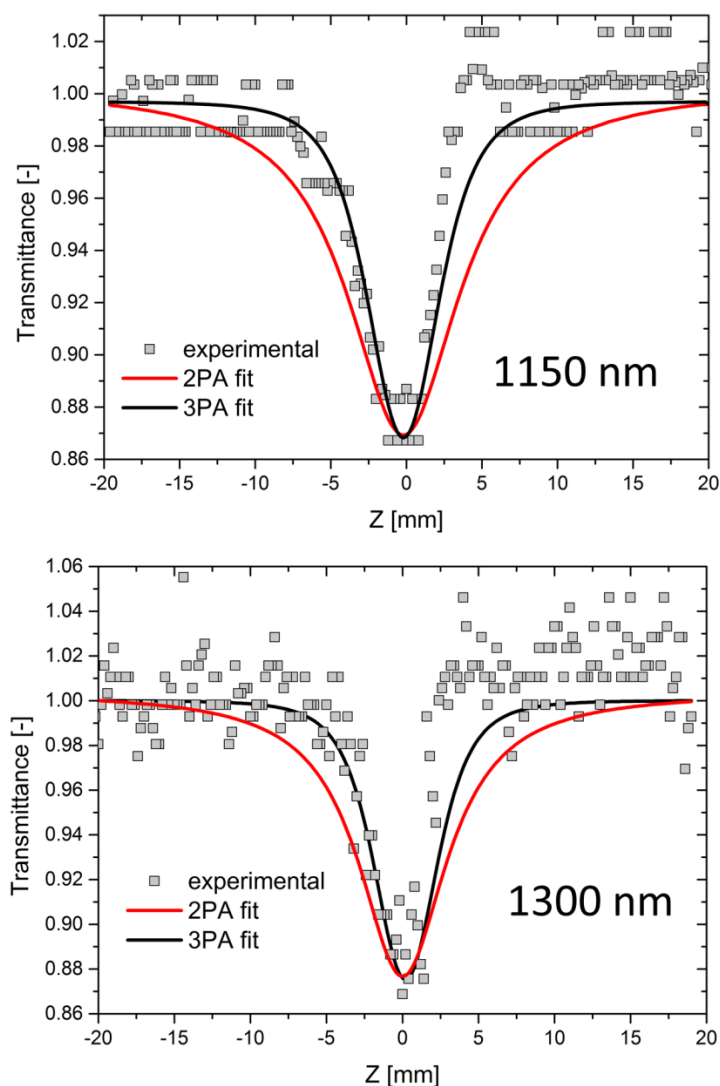


Fig. S15. Z-scan measurement traces at 1150 and 1300 nm for BHCVA in chloroform/acetone solution with 10% volume of acetone along with two-photon theoretical fit (red lines) and three-photon theoretical fit. In the case of no photochemical change the experimental traces should be vertically symmetric vs. $Z=0$.

The degradation of the dye upon prolonged irradiation was confirmed in a separate experiment, in which we irradiated the chloroform solution of **BHCVA** with high power (1W) 800 nm laser light directly from the regenerative amplifier for 3 hours. The photodegradation was evident, as judged from ^1H NMR spectroscopy (Fig. S16).

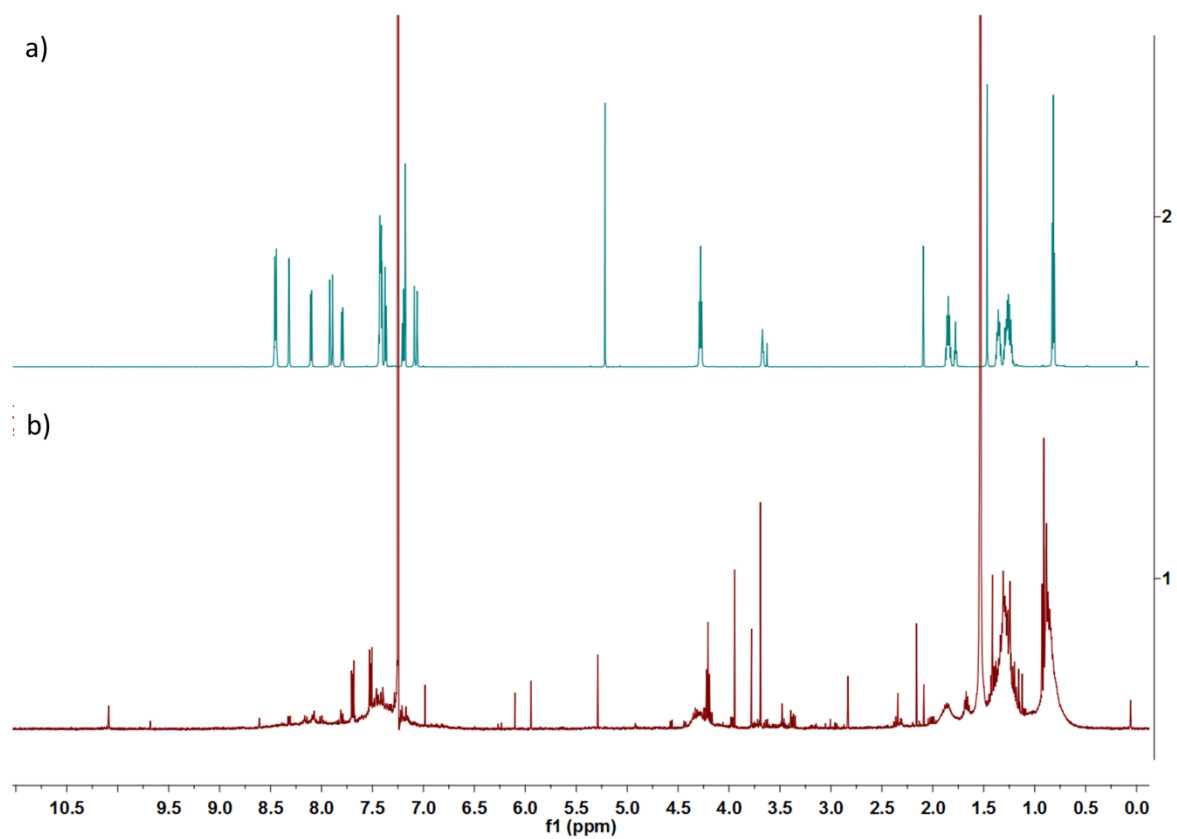


Fig. S16. A comparison of ^1H NMR (400 MHz, CDCl_3) spectra of a) pure BHCVA (before 800 nm irradiation), b) photochemically degraded BHCVA (after 800 nm irradiation).

Three-photon absorption cross section spectrum

Evaluation of nonlinear absorption properties in a range of wavelengths corresponding to the three-photon absorption (1100 – 1350 nm) was performed by obtaining a Z-scan from a selected region of solution twice. The second scan was obtained right after the first one to minimize effects resulting from diffusion of possible products of photochemical reactions. The OA traces obtained in the first scan were always asymmetric, strongly suggesting the presence of photochemically induced changes in the solution, whereas the OA traces obtained in the second scan were symmetric. Those symmetric traces were fitted with theoretical three-photon absorption curves. The three-photon absorption cross section spectra obtained in this manner for chloroform and chloroform/acetone mixtures did not exhibit any significant differences (Fig. S17). This result may indicate that the three-photon induced photochemical changes may influence the degree of aggregation but further comment is not possible without knowing the actual chemical identity of species that are produced upon irradiation in the 1100-1350 nm region and that give rise to the spectra in Fig. S17.

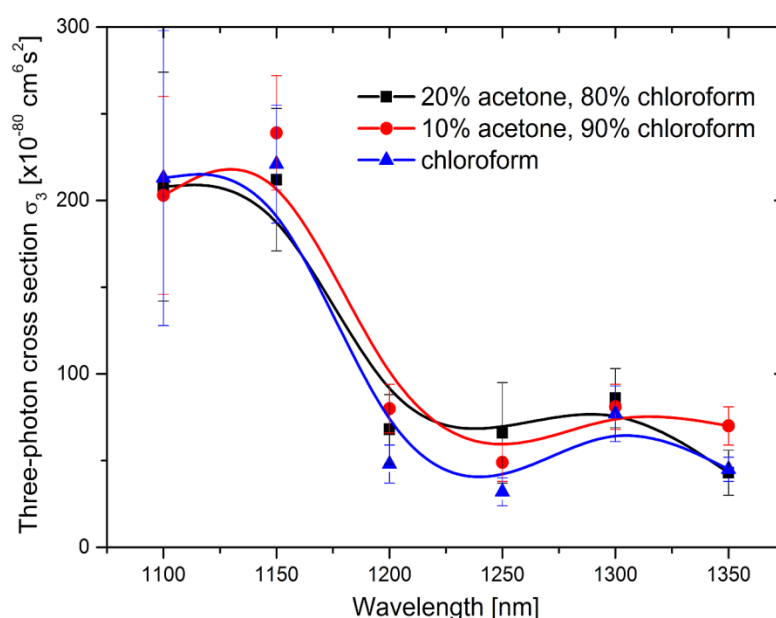
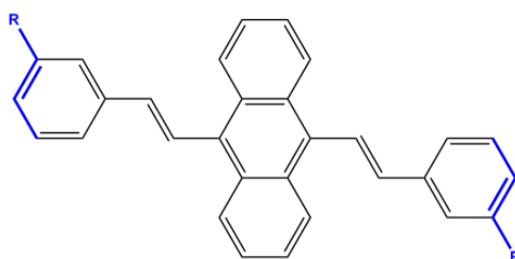


Fig. S17. Apparent three-photon cross section spectra of BHCVA in chloroform and chloroform/acetone solutions (10%, 20%). Full lines are drawn just to guide the eyes.

Aggregation motifs of molecules structurally related to BHCVA

Although at present it is not clear whether the structure of AIE aggregates corresponds to the structure of the crystalline solid, the X-ray crystal structures of AIE compounds, such as **BHCVA**, could be used as a valuable source of information on general trends on molecular self-assembly. Accordingly, a determination of recurrent structural motifs may allow for drawing probable aggregation models, necessary as starting points for electronic structure calculations of spectroscopic properties. Despite numerous trials, however, we were not able to obtain single crystals of **BHCVA** that could be used for X-ray diffraction studies. As a result, instead we surveyed CSD database (Web-based interface, February 2018) to establish what are structural preferences of molecules structurally related to **BHCVA**. Since a distinct feature of **BHCVA** is the protruding hexyl substituent, perpendicular to the main axis of the compound, we searched for crystal structures of similar compounds possessing functional group at the 3 position of the styryl fragment and/or ring expansion (see Scheme S1).



Scheme S1. Molecular structure used for CSD search. In blue are indicated atoms for which substructure search was performed

Database survey shows that there are no direct alkyl analogues of **BHCVA** deposited in the CSD. The most closely related compound to **BHCVA** is 3,3'-(anthracene-9,10-diyl)bis(10-hexyl-10*H*-phenothiazine), CSD refcode: VASKIL, which contains *N*-hexylphenothiazine fragment instead of *N*-hexylcarbazole one. As can be seen in Figure S18a there is a partial overlap between anthracene planes, which results in the stacking with offset along the anthracene fragment.

Exploration of crystal structures of the other 3-substituted styryl derivatives such as 9,10-bis(3,5-difluorostyryl)anthracene (ZEDJOJ), 9,10-bis(3,5-bis(trifluoromethyl)styryl)anthracene (ZEDJUP), 9,10-bis(3,5-dimethylstyryl)anthracene (ZEDKAW), 3,3'-(anthracene-9,10-diyl)bis(2,1-diyl)dibenzaldehyde (OPUGIR), 9,10-bis(2-(3-propoxyphenyl)vinyl)anthracene (DIGMAJ) shows formation of extensive offset π - π stacking as well. In those cases, also peripheral substituted styryl fragments are positioned in parallel (shown in Figure S18b, c, and d for selected examples). Note that all molecules are shifted along the short axis of the anthracene fragment. Taken together, we assumed that **BHCVA** molecule may assemble in the solid state according to the same pattern. The model based on the above analysis, used for electronic structure calculations, is referred to as “type B” in the main text of this paper.

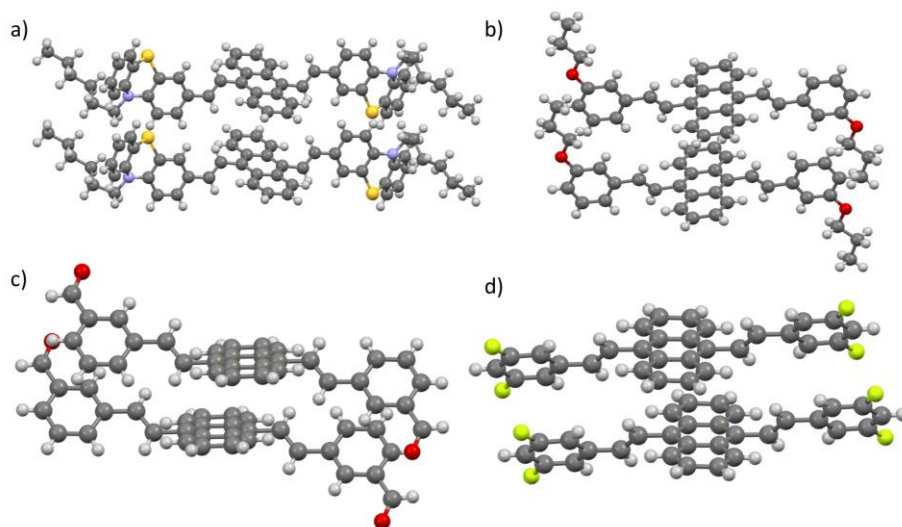


Figure S18. Visualizations of stacking patterns for structures of CSD reference codes a) VASKIL, b) DIGMAJ, c) OPUGIR and d) ZEDJUP.

Theoretical calculations

In this work we studied the electronic structure of monomer, dimer and trimer of 9,10-bis(*N*-hexylcarbazol-2-yl-vinyl-2)anthracene (hereafter abbreviated as **BHCVA**) using slightly simplified model (ethyl group instead of hexyl). Moreover, for aggregates we used two different types, denoted as A and B (see Fig. S19). All geometries were optimized *in vacuo* assuming C_i symmetry point group using 6-31G(d,p) basis set and B3LYP functional for monomer and BLYP-D2 functional for dimer and trimer. The GAUSSIAN program⁷ was used for this purpose. All geometries shown in Fig. S19 were confirmed to be true minima by evaluation of hessian.

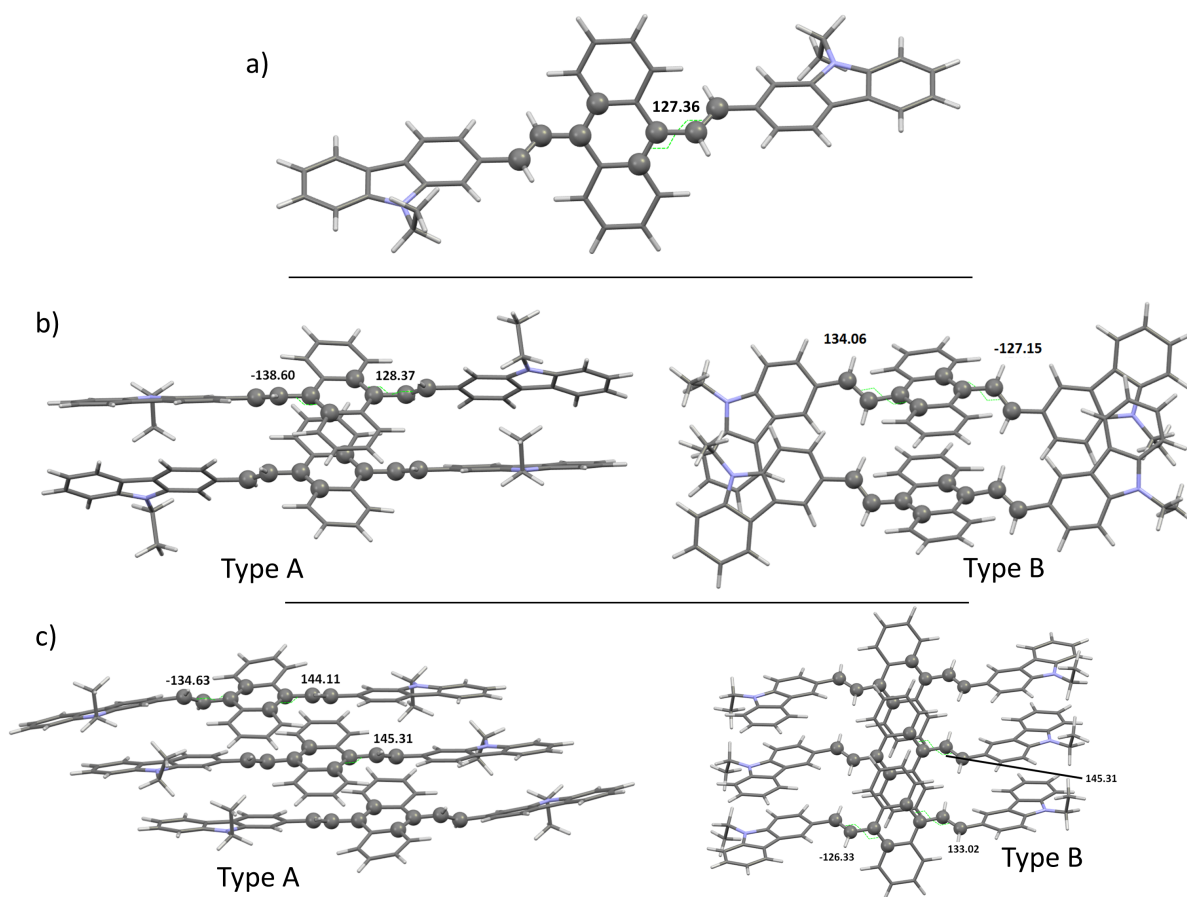


Fig. S19: a) Monomer, b) dimer (type A and B), and c) trimer (type A and B) optimized structures of BHCVA with indicated dihedral angles φ .

The results of electronic structure calculations, performed employing density functional theory for monomer, dimer and trimer assuming C_i symmetry point group and using the GAUSSIAN program, are reported in Tables S1–S17 (model A) and in Tables S22 and S23 (model B). When analyzing the performance of various density functionals (within model A) one can see that for each of the studied systems the range-separated functionals yield similar results and they predict, unlike B3LYP functional, that the maximum of one-photon excitation wavelength does not exceed 473 nm. The predictions of B3LYP are significantly overestimated. Hence, for further analysis, the CAM-B3LYP functional shall be employed. Moreover, there is only insignificant influence of solution environment on the optical spectra and the solvent-induced shifts for all electronic states do not exceed 12 nm. For this reason, gas-phase data are used to analyze electronic structure and two-photon absorption properties. The aggregation-induced changes in electronic structure are discussed in the manuscript.

We have also calculated the two-photon properties (TPA activity and TPA cross section) of the monomer, dimer and trimer using the DALTON program⁸. In the case of linearly polarized light, two-photon activity is given by:

$$\delta_{\text{TPA}} = \frac{1}{30} \sum_{\alpha\beta} [2S_{\alpha\alpha}S_{\beta\beta}^* + 2S_{\alpha\beta}S_{\alpha\beta}^* + 2S_{\alpha\beta}S_{\beta\alpha}^*], \quad (1)$$

where two-photon matrix elements, $S_{\alpha\alpha}$, for energy of incident photon ω_i are described as a summation running over intermediate states, i :

$$S_{\alpha\beta} = \sum_i \left(\frac{\langle 0|\mu_\alpha|i\rangle\langle i|\mu_\beta|f\rangle}{\omega_i - \frac{\omega_f}{2}} + \frac{\langle 0|\mu_\beta|i\rangle\langle i|\mu_\alpha|f\rangle}{\omega_i - \frac{\omega_f}{2}} \right) \quad (2)$$

Note that by symmetry:

$$\begin{aligned} \langle A_g|\hat{\mu}|A_g\rangle &= 0 \\ \langle A_g|\hat{\mu}|A_u\rangle &\neq 0 \end{aligned}$$

δ_{TPA} can be related to experimentally measured TPA cross sections using the following equation:

$$\sigma_2(\omega) = \frac{4\pi^3\alpha a_0^5\omega^2}{c} g(2\omega) \delta_{\text{TPA}} \quad (3)$$

where $g(2\omega)$ is the line shape function, a_0 is the Bohr radius, α is the fine structure constant, c is the speed of the light. In our studies we used a normalized Gauss function as a line shape function with a broadening parameter, Γ_f , equal to 0.50 eV. The final expression of TPA cross section in the maximum of the band reads:

$$\sigma_2(\omega = \frac{1}{2}\omega_f) = \frac{8\pi^3\sqrt{2\ln 2}\alpha a_0^5\omega^2}{c\Gamma_f\sqrt{2\pi}} \delta_{\text{TPA}}. \quad (4)$$

The results of calculations of two-photon absorption properties are presented in Tables S18–S20 (model A) and in Tables S24 and S25 (model B). In order to gain an insight into aggregation-induced increase in TPA intensity we performed an analysis of electronic structure parameters (transition moments and excitation energies) for monomer and dimer (model A), and the data are collected in Table S21. The obtained results are discussed in the manuscript.

Table S1: One-photon absorption spectra of monomer *in vacuo* determined at the B3LYP/6-31G(d,p) level of theory.

| | Symmetry | ΔE_{vert} [eV] | λ_{vert} [nm] | f |
|---|----------|-------------------------------|------------------------------|--------|
| 1 | A_u | 2.5842 | 479.78 | 1.0695 |
| 2 | A_g | 3.1979 | 387.70 | 0.0000 |
| 2 | A_u | 3.1996 | 387.50 | 0.0136 |
| 3 | A_g | 3.2068 | 386.63 | 0.0000 |
| 3 | A_u | 3.2867 | 377.23 | 0.0187 |
| 4 | A_g | 3.3804 | 366.78 | 0.0000 |
| 4 | A_u | 3.4789 | 356.39 | 0.3195 |
| 5 | A_u | 3.6867 | 336.30 | 0.0002 |
| 6 | A_u | 3.8385 | 323.00 | 0.0404 |
| 5 | A_g | 3.8386 | 323.00 | 0.0000 |
| 7 | A_u | 4.1283 | 300.33 | 0.8100 |
| 6 | A_g | 4.1918 | 295.78 | 0.0000 |
| 7 | A_g | 4.1939 | 295.63 | 0.0000 |
| 8 | A_u | 4.1946 | 295.58 | 0.0079 |
| 8 | A_g | 4.2366 | 292.65 | 0.0000 |

Table S2: One-photon absorption spectra of monomer *in vacuo* determined at the ω B97X-D/6-31G(d,p) level of theory.

| | Symmetry | ΔE_{vert} [eV] | λ_{vert} [nm] | f |
|---|----------|-------------------------------|------------------------------|--------|
| 1 | A_u | 3.0305 | 409.12 | 1.1367 |
| 2 | A_u | 3.9325 | 315.28 | 0.0006 |
| 2 | A_g | 4.1279 | 300.36 | 0.0000 |
| 3 | A_u | 4.1284 | 300.32 | 0.0737 |
| 3 | A_g | 4.1545 | 298.43 | 0.0000 |
| 4 | A_u | 4.1600 | 298.04 | 1.2118 |
| 5 | A_u | 4.4748 | 277.07 | 0.0649 |
| 4 | A_g | 4.5250 | 274.00 | 0.0000 |
| 6 | A_u | 4.8367 | 256.34 | 0.0106 |
| 5 | A_g | 4.8644 | 254.88 | 0.0000 |
| 6 | A_g | 5.0038 | 247.78 | 0.0000 |
| 7 | A_u | 5.1798 | 239.36 | 1.2193 |
| 7 | A_g | 5.2441 | 236.43 | 0.0000 |
| 8 | A_u | 5.2670 | 235.40 | 0.0793 |
| 8 | A_g | 5.2733 | 235.12 | 0.0000 |

Table S3: One-photon absorption spectra of monomer *in vacuo* determined at the BHandHLYP/6-31G(d,p) level of theory.

| | Symmetry | ΔE_{vert} [eV] | λ_{vert} [nm] | f |
|---|----------|-------------------------------|------------------------------|--------|
| 1 | A_u | 2.9826 | 415.70 | 1.2110 |
| 2 | A_u | 4.0120 | 309.03 | 0.0113 |
| 2 | A_g | 4.0430 | 306.66 | 0.0000 |
| 3 | A_u | 4.0659 | 304.94 | 0.9357 |
| 3 | A_g | 4.1638 | 297.77 | 0.0000 |
| 4 | A_u | 4.1645 | 297.72 | 0.0830 |
| 4 | A_g | 4.2095 | 294.53 | 0.0000 |
| 5 | A_u | 4.2567 | 291.27 | 0.0865 |
| 6 | A_u | 4.7410 | 261.51 | 0.1852 |
| 5 | A_g | 4.7858 | 259.07 | 0.0000 |
| 7 | A_u | 4.8446 | 255.92 | 0.0506 |
| 6 | A_g | 4.8471 | 255.79 | 0.0000 |
| 7 | A_g | 5.0068 | 247.63 | 0.0000 |
| 8 | A_u | 5.1957 | 238.63 | 1.0881 |
| 8 | A_g | 5.2098 | 237.98 | 0.0000 |

Table S4: One-photon absorption spectra of monomer *in vacuo* determined at the CAM-B3LYP/6-31G(d,p) level of theory.

| | Symmetry | ΔE_{vert} [eV] | λ_{vert} [nm] | f | orb. transitions |
|---|----------|-------------------------------|------------------------------|--------|------------------------------|
| 1 | A_u | 2.9932 | 414.22 | 1.1547 | HOMO→LUMO |
| 2 | A_u | 3.9210 | 316.21 | 0.0012 | HOMO-5→LUMO, HOMO→LUMO+3 |
| 2 | A_g | 4.0679 | 304.79 | 0.0000 | HOMO-3→LUMO, HOMO→LUMO+1 |
| 3 | A_g | 4.0796 | 303.92 | 0.0000 | HOMO-2→LUMO+1, HOMO-1→LUMO |
| 3 | A_u | 4.0797 | 303.90 | 0.1229 | HOMO-2→LUMO, HOMO-1→LUMO+1 |
| 4 | A_u | 4.0864 | 303.41 | 0.9782 | HOMO→LUMO+2, |
| 4 | A_g | 4.2911 | 288.93 | 0.0000 | HOMO-3→LUMO, HOMO→LUMO+1 |
| 5 | A_u | 4.3054 | 287.97 | 0.0883 | HOMO-4→LUMO |
| 6 | A_u | 4.7452 | 261.28 | 0.0756 | HOMO-4→LUMO+2, HOMO-3→LUMO+1 |
| 5 | A_g | 4.7764 | 259.58 | 0.0000 | HOMO-4→LUMO+1, HOMO-3→LUMO+2 |
| 7 | A_u | 4.9330 | 251.34 | 0.0788 | HOMO-2→LUMO |
| 6 | A_g | 4.9363 | 251.17 | 0.0000 | HOMO-1→LUMO |
| 7 | A_g | 4.9703 | 249.45 | 0.0000 | HOMO-6→LUMO |
| 8 | A_u | 5.1416 | 241.14 | 1.1409 | HOMO-5→LUMO, HOMO→LUMO+3 |
| 8 | A_g | 5.1557 | 240.48 | 0.0000 | HOMO→LUMO+8 |

Table S5: One-photon absorption spectra of monomer in CHCl₃ solution determined at the CAM-B3LYP/6-31G(d,p) level of theory. Solvent effects were included using PCM method.

| | Symmetry | ΔE_{vert} [eV] | λ_{vert} [nm] | f |
|---|----------------|-------------------------------|------------------------------|--------|
| 1 | A _u | 2.9281 | 423.43 | 1.2751 |
| 2 | A _u | 3.9223 | 316.10 | 0.0032 |
| 2 | A _g | 3.9818 | 311.38 | 0.0000 |
| 3 | A _g | 4.0359 | 307.20 | 0.0000 |
| 3 | A _u | 4.0361 | 307.19 | 0.1343 |
| 4 | A _u | 4.0484 | 306.26 | 1.2070 |
| 4 | A _g | 4.2947 | 288.69 | 0.0000 |
| 5 | A _u | 4.3002 | 288.32 | 0.0313 |
| 6 | A _u | 4.7200 | 262.68 | 0.0968 |
| 5 | A _g | 4.7522 | 260.90 | 0.0000 |
| 7 | A _u | 4.8669 | 254.75 | 0.1039 |
| 6 | A _g | 4.8707 | 254.55 | 0.0000 |
| 8 | A _u | 4.9581 | 250.06 | 1.5224 |
| 7 | A _g | 4.9619 | 249.87 | 0.0000 |
| 7 | A _g | 5.1462 | 240.92 | 0.0000 |

Table S6: Frontier orbitals involved in one-photon transitions. All calculations were performed at the CAM-B3LYP level of theory. See Table 4 for orbital assignments.

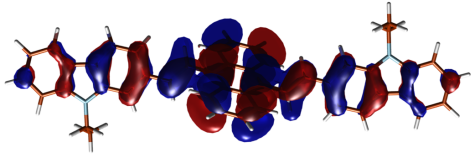
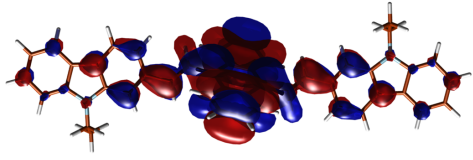
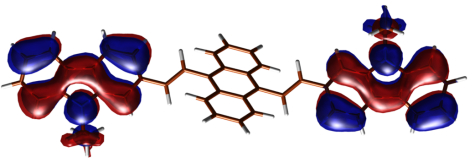
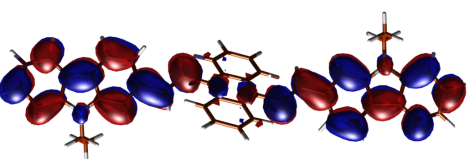
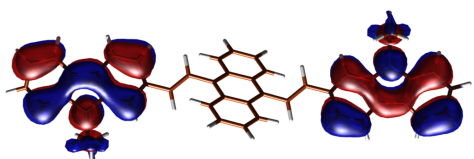
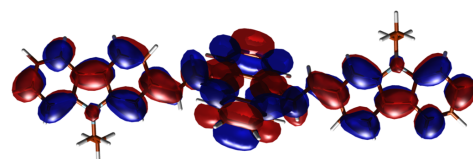
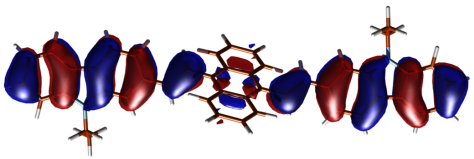
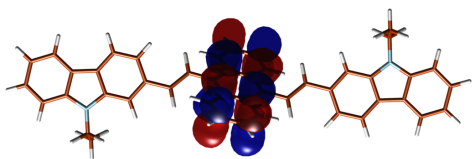
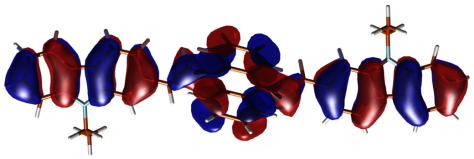
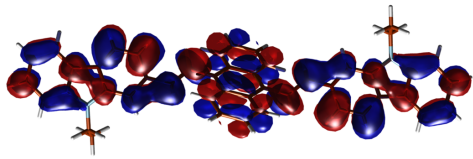
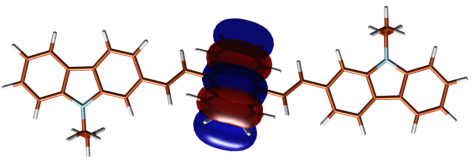
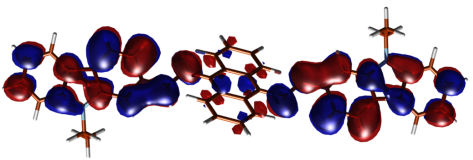
| | |
|--|---|
| <p>HOMO</p>  | <p>LUMO</p>  |
| <p>HOMO-1</p>  | <p>LUMO+1</p>  |
| <p>HOMO-2</p>  | <p>LUMO+2</p>  |
| <p>HOMO-3</p>  | <p>LUMO+3</p>  |
| <p>HOMO-4</p>  | <p>LUMO+4</p>  |
| <p>HOMO-5</p>  | <p>LUMO+5</p>  |

Table S7: One-photon absorption spectra of dimer (model A) *in vacuo* determined at the B3LYP/6-31G(d,p) level of theory.

| | Symmetry | ΔE_{vert} [eV] | λ_{vert} [nm] | f |
|----|----------|-------------------------------|------------------------------|--------|
| 2 | A_g | 2.0978 | 591.02 | 0.0000 |
| 1 | A_u | 2.1250 | 583.45 | 0.2809 |
| 3 | A_g | 2.3604 | 525.27 | 0.0000 |
| 2 | A_u | 2.5337 | 489.34 | 1.7911 |
| 4 | A_g | 2.9416 | 421.48 | 0.0000 |
| 3 | A_u | 2.9560 | 419.43 | 0.0061 |
| 4 | A_u | 2.9602 | 418.84 | 0.0097 |
| 5 | A_g | 2.9739 | 416.91 | 0.0000 |
| 5 | A_u | 2.9746 | 416.81 | 0.0013 |
| 6 | A_g | 2.9942 | 414.08 | 0.0000 |
| 6 | A_u | 3.0110 | 411.77 | 0.0136 |
| 7 | A_g | 3.0305 | 409.12 | 0.0000 |
| 8 | A_g | 3.0508 | 406.40 | 0.0000 |
| 7 | A_u | 3.0535 | 406.04 | 0.0358 |
| 8 | A_u | 3.1318 | 395.89 | 0.1404 |
| 9 | A_g | 3.1326 | 395.79 | 0.0000 |
| 9 | A_u | 3.1686 | 391.29 | 0.0059 |
| 10 | A_g | 3.1688 | 391.27 | 0.0000 |
| 10 | A_u | 3.2028 | 387.11 | 0.0051 |
| 11 | A_g | 3.2057 | 386.77 | 0.0000 |

Table S8: One-photon absorption spectra of dimer (model A) *in vacuo* determined at the ω B97X-D/6-31G(d,p) level of theory.

| | Symmetry | ΔE_{vert} [eV] | λ_{vert} [nm] | f |
|----|----------|-------------------------------|------------------------------|--------|
| 2 | A_g | 2.6695 | 464.44 | 0.0000 |
| 1 | A_u | 2.8233 | 439.15 | 1.7717 |
| 3 | A_g | 3.2090 | 386.36 | 0.0000 |
| 2 | A_u | 3.2488 | 381.63 | 0.4603 |
| 3 | A_u | 3.7712 | 328.77 | 0.0047 |
| 4 | A_u | 3.8025 | 326.06 | 0.0020 |
| 4 | A_g | 3.8100 | 325.41 | 0.0000 |
| 5 | A_g | 3.8830 | 319.30 | 0.0000 |
| 5 | A_u | 3.9654 | 312.67 | 0.0179 |
| 6 | A_g | 3.9666 | 312.57 | 0.0000 |
| 6 | A_u | 3.9902 | 310.72 | 1.1023 |
| 7 | A_g | 3.9966 | 310.22 | 0.0000 |
| 7 | A_u | 4.0262 | 307.94 | 0.7325 |
| 8 | A_g | 4.0320 | 307.50 | 0.0000 |
| 9 | A_g | 4.2544 | 291.42 | 0.0000 |
| 8 | A_u | 4.2644 | 290.74 | 0.1507 |
| 10 | A_g | 4.2870 | 289.21 | 0.0000 |
| 9 | A_u | 4.3032 | 288.12 | 0.0084 |
| 11 | A_g | 4.4364 | 279.47 | 0.0000 |
| 10 | A_u | 4.4375 | 279.40 | 0.0272 |

Table S9: One-photon absorption spectra of dimer (model A) *in vacuo* determined at the BHandHLYP/6-31G(d,p) level of theory.

| | Symmetry | ΔE_{vert} [eV] | λ_{vert} [nm] | f |
|----|----------|-------------------------------|------------------------------|--------|
| 2 | A_g | 2.5973 | 477.36 | 0.0000 |
| 1 | A_u | 2.7347 | 453.37 | 1.5395 |
| 3 | A_g | 3.0258 | 409.76 | 0.0000 |
| 2 | A_u | 3.0895 | 401.30 | 0.8466 |
| 3 | A_u | 3.6528 | 339.42 | 0.0045 |
| 4 | A_g | 3.7741 | 328.51 | 0.0000 |
| 5 | A_g | 3.8594 | 321.25 | 0.0000 |
| 4 | A_u | 3.8602 | 321.18 | 0.5082 |
| 6 | A_g | 3.8779 | 319.72 | 0.0000 |
| 5 | A_u | 3.8798 | 319.56 | 0.6037 |
| 7 | A_g | 3.9402 | 314.66 | 0.0000 |
| 6 | A_u | 3.9500 | 313.89 | 0.0140 |
| 7 | A_u | 3.9579 | 313.25 | 0.0605 |
| 8 | A_g | 3.9614 | 312.98 | 0.0000 |
| 9 | A_g | 4.0043 | 309.62 | 0.0000 |
| 8 | A_u | 4.0065 | 309.46 | 0.0814 |
| 9 | A_u | 4.0279 | 307.81 | 0.2408 |
| 10 | A_g | 4.0315 | 307.54 | 0.0000 |
| 11 | A_g | 4.1640 | 297.76 | 0.0000 |
| 10 | A_u | 4.1648 | 297.70 | 0.0753 |

Table S10: One-photon absorption spectra of dimer (model A) *in vacuo* determined at the CAM-B3LYP/6-31G(d,p) level of theory.

| | Symmetry | ΔE_{vert} [eV] | λ_{vert} [nm] | f | orb. transitions |
|----|----------|-------------------------------|------------------------------|--------|---|
| 2 | A_g | 2.6232 | 472.65 | 0.0000 | HOMO-1 \rightarrow LUMO, HOMO \rightarrow LUMO+1 |
| 1 | A_u | 2.7625 | 448.81 | 1.5832 | HOMO \rightarrow LUMO |
| 3 | A_g | 3.0721 | 403.58 | 0.0000 | HOMO-1 \rightarrow LUMO, HOMO \rightarrow LUMO+1 |
| 2 | A_u | 3.1275 | 396.44 | 0.6843 | HOMO-1 \rightarrow LUMO+1 |
| 3 | A_u | 3.6861 | 336.35 | 0.0048 | HOMO-2 \rightarrow LUMO+1, HOMO \rightarrow LUMO+3 |
| 4 | A_u | 3.7848 | 327.58 | 0.0046 | HOMO-11 \rightarrow LUMO+1, HOMO-10 \rightarrow LUMO HOMO \rightarrow LUMO+7 |
| 4 | A_g | 3.7855 | 327.52 | 0.0000 | HOMO \rightarrow LUMO+5, HOMO \rightarrow LUMO+6 |
| 5 | A_g | 3.8146 | 325.03 | 0.0000 | HOMO \rightarrow LUMO+2 |
| 6 | A_g | 3.9019 | 317.75 | 0.0000 | HOMO-2 \rightarrow LUMO, HOMO \rightarrow LUMO+2 |
| 5 | A_u | 3.9040 | 317.59 | 0.3806 | HOMO-3 \rightarrow LUMO |
| 6 | A_u | 3.9051 | 317.49 | 0.7991 | HOMO \rightarrow LUMO+4 |
| 7 | A_g | 3.9070 | 317.34 | 0.0000 | HOMO-4 \rightarrow LUMO |
| 8 | A_g | 3.9553 | 313.46 | 0.0000 | HOMO-3 \rightarrow LUMO+1 |
| 7 | A_u | 3.9565 | 313.37 | 0.2747 | HOMO-4 \rightarrow LUMO+1 |
| 9 | A_g | 4.0393 | 306.95 | 0.0000 | HOMO-2 \rightarrow LUMO, HOMO \rightarrow LUMO+2 |
| 8 | A_u | 4.0562 | 305.67 | 0.0232 | HOMO-2 \rightarrow LUMO+1, HOMO \rightarrow LUMO+3 |
| 10 | A_g | 4.0884 | 303.26 | 0.0000 | HOMO-5 \rightarrow LUMO+1 |
| 9 | A_u | 4.0905 | 303.10 | 0.2124 | HOMO-5 \rightarrow LUMO |
| 11 | A_g | 4.2379 | 292.56 | 0.0000 | HOMO-1 \rightarrow LUMO+3 |
| 10 | A_u | 4.2388 | 292.50 | 0.0496 | HOMO-1 \rightarrow LUMO+2 |

Table S11: One-photon absorption spectra of dimer (model A) in CHCl_3 solution determined at the CAM-B3LYP/6-31G(d,p) level of theory. Solvent effects were included using PCM method.

| | Symmetry | ΔE_{vert} [eV] | λ_{vert} [nm] | f |
|----|----------|-------------------------------|------------------------------|--------|
| 2 | A_g | 2.6033 | 476.26 | 0.0000 |
| 1 | A_u | 2.6961 | 459.86 | 2.0863 |
| 3 | A_g | 3.0653 | 404.48 | 0.0000 |
| 2 | A_u | 3.1040 | 399.44 | 0.6247 |
| 3 | A_u | 3.6632 | 338.46 | 0.0058 |
| 4 | A_g | 3.7794 | 328.06 | 0.0000 |
| 4 | A_u | 3.7843 | 327.63 | 0.0119 |
| 5 | A_g | 3.8066 | 325.71 | 0.0000 |
| 6 | A_g | 3.8197 | 324.59 | 0.0000 |
| 5 | A_u | 3.8701 | 320.36 | 0.0901 |
| 7 | A_g | 3.8726 | 320.16 | 0.0000 |
| 6 | A_u | 3.8735 | 320.08 | 1.4337 |
| 8 | A_g | 3.9140 | 316.77 | 0.0000 |
| 7 | A_u | 3.9173 | 316.51 | 0.3449 |
| 9 | A_g | 4.0386 | 307.00 | 0.0000 |
| 8 | A_u | 4.0549 | 305.76 | 0.0185 |
| 9 | A_u | 4.0802 | 303.87 | 0.1213 |
| 10 | A_g | 4.0805 | 303.85 | 0.0000 |
| 11 | A_g | 4.2369 | 292.63 | 0.0000 |
| 10 | A_u | 4.2423 | 292.26 | 0.0365 |

Table S12: Frontier orbitals involved in one-photon transitions. All calculations were performed at the CAM-B3LYP level of theory. See Table 10 for orbital assignments.

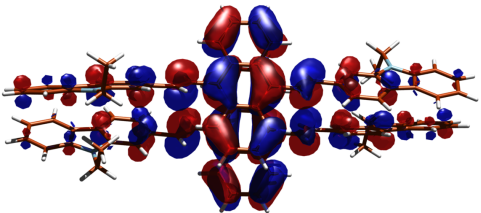
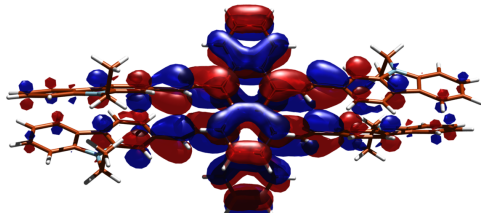
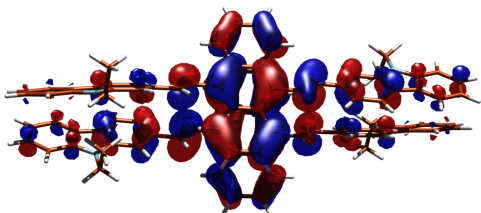
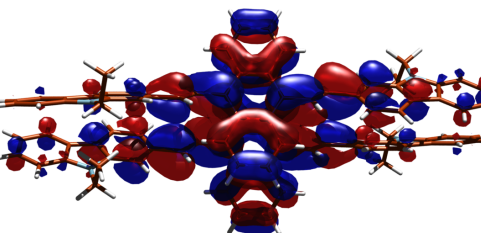
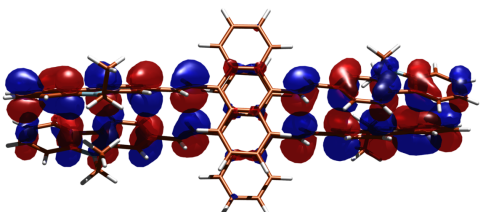
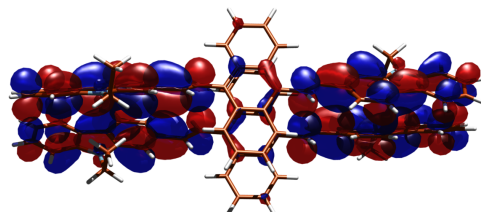
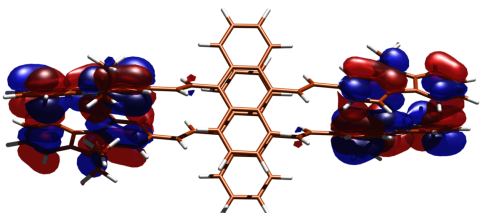
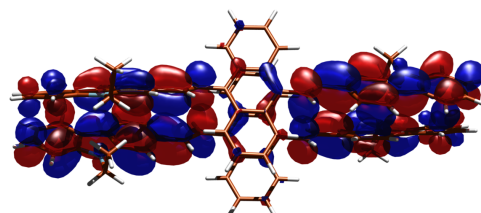
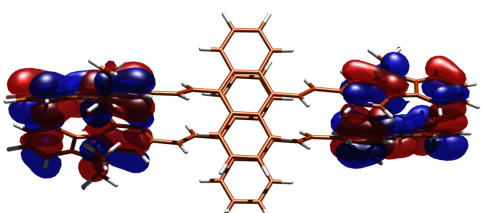
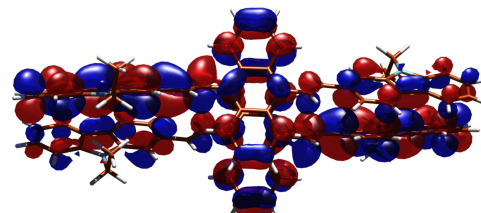
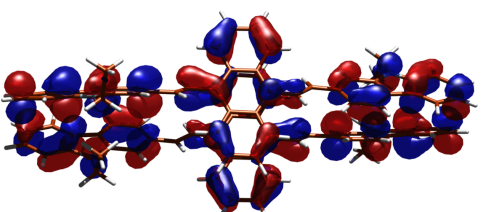
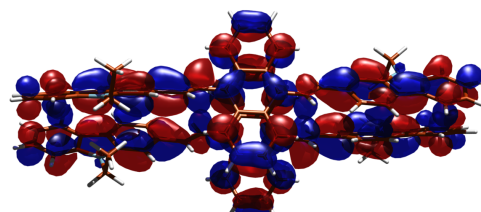
| | |
|--|---|
| <p>HOMO</p>  | <p>LUMO</p>  |
| <p>HOMO-1</p>  | <p>LUMO+1</p>  |
| <p>HOMO-2</p>  | <p>LUMO+2</p>  |
| <p>HOMO-3</p>  | <p>LUMO+3</p>  |
| <p>HOMO-4</p>  | <p>LUMO+4</p>  |
| <p>HOMO-5</p>  | <p>LUMO+5</p>  |

Table S13: One-photon absorption spectra of trimer (model A) *in vacuo* determined at B3LYP/6-31G(d,p) level of theory.

| | Symmetry | ΔE_{vert} [eV] | λ_{vert} [nm] | f |
|----|----------|-------------------------------|------------------------------|--------|
| 2 | A_g | 1.9317 | 641.84 | 0.0000 |
| 1 | A_u | 1.9326 | 641.54 | 0.0104 |
| 2 | A_u | 1.9757 | 627.53 | 0.3312 |
| 3 | A_g | 2.1608 | 573.79 | 0.0000 |
| 3 | A_u | 2.2826 | 543.18 | 0.0724 |
| 4 | A_g | 2.3134 | 535.93 | 0.0000 |
| 4 | A_u | 2.3846 | 519.94 | 0.3974 |
| 5 | A_g | 2.4188 | 512.58 | 0.0000 |
| 5 | A_u | 2.4906 | 497.82 | 1.7054 |
| 6 | A_g | 2.6727 | 463.89 | 0.0000 |
| 6 | A_u | 2.6911 | 460.71 | 0.0060 |
| 7 | A_g | 2.7022 | 458.82 | 0.0000 |
| 7 | A_u | 2.7451 | 451.66 | 0.0019 |
| 8 | A_g | 2.7881 | 444.69 | 0.0000 |
| 8 | A_u | 2.7956 | 443.50 | 0.0126 |
| 9 | A_g | 2.7972 | 443.24 | 0.0000 |
| 9 | A_u | 2.8496 | 435.09 | 0.0054 |
| 10 | A_g | 2.8527 | 434.61 | 0.0000 |
| 10 | A_u | 2.8695 | 432.07 | 0.0214 |
| 11 | A_u | 2.8786 | 430.71 | 0.1216 |

Table S14: One-photon absorption spectra of trimer (model A) *in vacuo* determined at ω B97X-D/6-31G(d,p) level of theory.

| | Symmetry | ΔE_{vert} [eV] | λ_{vert} [nm] | f |
|----|----------|-------------------------------|------------------------------|--------|
| 1 | A_u | 2.4839 | 499.15 | 0.1482 |
| 2 | A_g | 2.6595 | 466.20 | 0.0000 |
| 2 | A_u | 2.7374 | 452.93 | 2.0037 |
| 3 | A_g | 3.1301 | 396.10 | 0.0000 |
| 3 | A_u | 3.1362 | 395.33 | 0.3657 |
| 4 | A_g | 3.1999 | 387.47 | 0.0000 |
| 4 | A_u | 3.2796 | 378.05 | 0.2867 |
| 5 | A_u | 3.7024 | 334.88 | 0.0078 |
| 5 | A_g | 3.7147 | 333.77 | 0.0000 |
| 6 | A_u | 3.7548 | 330.21 | 0.0051 |
| 6 | A_g | 3.7712 | 328.76 | 0.0000 |
| 7 | A_u | 3.7804 | 327.96 | 0.4001 |
| 7 | A_g | 3.8631 | 320.95 | 0.0000 |
| 8 | A_u | 3.9253 | 315.86 | 0.2070 |
| 8 | A_g | 3.9326 | 315.27 | 0.0000 |
| 9 | A_u | 3.9361 | 314.99 | 0.3885 |
| 9 | A_g | 3.9417 | 314.54 | 0.0000 |
| 10 | A_u | 3.9583 | 313.22 | 1.3751 |
| 11 | A_u | 3.9694 | 312.35 | 0.0612 |
| 10 | A_g | 3.9864 | 311.02 | 0.0000 |

Table S15: One-photon absorption spectra of trimer (model A) *in vacuo* determined at BHandHLYP/6-31G(d,p) level of theory.

| | Symmetry | ΔE_{vert} [eV] | λ_{vert} [nm] | f |
|----|----------|-------------------------------|------------------------------|--------|
| 1 | A_u | 2.4059 | 515.34 | 0.1469 |
| 2 | A_g | 2.5604 | 484.24 | 0.0000 |
| 2 | A_u | 2.6240 | 472.50 | 1.4906 |
| 3 | A_g | 2.8926 | 428.63 | 0.0000 |
| 3 | A_u | 2.9225 | 424.25 | 0.7918 |
| 4 | A_g | 2.9715 | 417.25 | 0.0000 |
| 4 | A_u | 3.0721 | 403.59 | 0.5520 |
| 5 | A_u | 3.5296 | 351.27 | 0.0048 |
| 5 | A_g | 3.5335 | 350.88 | 0.0000 |
| 6 | A_g | 3.5363 | 350.60 | 0.0000 |
| 6 | A_u | 3.5911 | 345.26 | 0.1653 |
| 7 | A_g | 3.6350 | 341.09 | 0.0000 |
| 7 | A_u | 3.6902 | 335.98 | 0.4026 |
| 8 | A_u | 3.7570 | 330.00 | 0.0288 |
| 9 | A_u | 3.7655 | 329.27 | 0.4845 |
| 8 | A_g | 3.7907 | 327.07 | 0.0000 |
| 9 | A_g | 3.8102 | 325.40 | 0.0000 |
| 10 | A_u | 3.8212 | 324.46 | 0.4746 |
| 10 | A_g | 3.8256 | 324.09 | 0.0000 |
| 11 | A_u | 3.8453 | 322.43 | 0.1298 |

Table S16: One-photon absorption spectra of trimer (model A) *in vacuo* determined at CAM-B3LYP/6-31G(d,p) level of theory.

| | Symmetry | ΔE_{vert} [eV] | λ_{vert} [nm] | f |
|----|----------|-------------------------------|------------------------------|--------|
| 1 | A_u | 2.4338 | 509.42 | 0.1449 |
| 2 | A_g | 2.5967 | 477.47 | 0.0000 |
| 2 | A_u | 2.6655 | 465.14 | 1.6731 |
| 3 | A_g | 2.9619 | 418.60 | 0.0000 |
| 3 | A_u | 2.9820 | 415.77 | 0.6024 |
| 4 | A_g | 3.0361 | 408.36 | 0.0000 |
| 4 | A_u | 3.1269 | 396.51 | 0.4238 |
| 5 | A_g | 3.5932 | 345.05 | 0.0000 |
| 5 | A_u | 3.6274 | 341.80 | 0.0954 |
| 6 | A_u | 3.6903 | 335.97 | 0.2232 |
| 6 | A_g | 3.7029 | 334.83 | 0.0000 |
| 7 | A_u | 3.7232 | 333.01 | 0.0611 |
| 7 | A_g | 3.7397 | 331.54 | 0.0000 |
| 8 | A_g | 3.7581 | 329.91 | 0.0000 |
| 8 | A_u | 3.7582 | 329.90 | 0.0957 |
| 9 | A_u | 3.7971 | 326.53 | 0.2757 |
| 10 | A_u | 3.8283 | 323.86 | 0.4384 |
| 9 | A_g | 3.8360 | 323.21 | 0.0000 |
| 10 | A_g | 3.8546 | 321.65 | 0.0000 |
| 11 | A_u | 3.8712 | 320.28 | 0.5482 |

Table S17: One-photon absorption spectra of trimer (model A) in CHCl_3 determined at CAM-B3LYP/6-31G(d,p) level of theory. Solvent effects were included using PCM method.

| | Symmetry | ΔE_{vert} [eV] | λ_{vert} [nm] | f |
|----|----------|-------------------------------|------------------------------|--------|
| 1 | A_u | 2.4192 | 512.50 | 0.2884 |
| 2 | A_g | 2.5619 | 483.96 | 0.0000 |
| 2 | A_u | 2.6002 | 476.82 | 2.1712 |
| 3 | A_g | 2.9189 | 424.76 | 0.0000 |
| 3 | A_u | 2.9308 | 423.03 | 0.8430 |
| 4 | A_g | 3.0680 | 404.12 | 0.0000 |
| 4 | A_u | 3.1477 | 393.89 | 0.3304 |
| 5 | A_g | 3.5560 | 348.66 | 0.0000 |
| 5 | A_u | 3.5869 | 345.66 | 0.1150 |
| 6 | A_g | 3.6426 | 340.37 | 0.0000 |
| 6 | A_u | 3.6836 | 336.59 | 0.3292 |
| 7 | A_u | 3.7161 | 333.64 | 0.1753 |
| 7 | A_g | 3.7371 | 331.77 | 0.0000 |
| 8 | A_u | 3.7443 | 331.13 | 0.0450 |
| 8 | A_g | 3.7477 | 330.83 | 0.0000 |
| 9 | A_u | 3.7678 | 329.06 | 0.4176 |
| 10 | A_u | 3.7958 | 326.64 | 0.3805 |
| 9 | A_g | 3.8004 | 326.24 | 0.0000 |
| 10 | A_g | 3.8164 | 324.87 | 0.0000 |
| 11 | A_u | 3.8282 | 323.87 | 0.4157 |

Table S18: Summary of CAM-B3LYP/6-31G(d,p) calculations of TPA properties for monomer *in vacuo*.

| | Symmetry | ΔE_{vert} [eV] | λ_{vert} [nm] | δ^{TPA} [au] | σ^{TPA} [GM] |
|---|----------|-------------------------------|------------------------------|----------------------------|----------------------------|
| 2 | A_g | 4.07 | 304.79 | 0.611×10^3 | 2 |
| 3 | A_g | 4.08 | 303.92 | 0.345×10^4 | 12 |
| 4 | A_g | 4.29 | 288.93 | 0.446×10^6 | 1773 |
| 5 | A_g | 4.78 | 259.58 | 0.107×10^4 | 5 |
| 6 | A_g | 4.94 | 251.17 | 0.222×10^4 | 12 |
| 7 | A_g | 4.97 | 249.45 | 0.132×10^5 | 70 |
| 8 | A_g | 5.16 | 240.48 | 0.412×10^5 | 237 |

Table S19: Summary of CAM-B3LYP/6-31G(d,p) calculations of TPA properties for dimer (model A) *in vacuo*.

| | Symmetry | ΔE_{vert} [eV] | λ_{vert} [nm] | δ^{TPA} [au] | σ^{TPA} [GM] |
|----|----------|-------------------------------|------------------------------|----------------------------|----------------------------|
| 2 | A_g | 2.62 | 472.65 | 0.176×10^3 | <1 |
| 3 | A_g | 3.07 | 403.58 | 0.117×10^4 | 2 |
| 4 | A_g | 3.79 | 327.52 | 0.235×10^4 | 7 |
| 5 | A_g | 3.81 | 325.03 | 0.813×10^3 | 3 |
| 6 | A_g | 3.90 | 317.75 | 0.145×10^4 | 5 |
| 7 | A_g | 3.90 | 317.34 | 0.311×10^4 | 10 |
| 8 | A_g | 3.95 | 313.46 | 0.167×10^5 | 56 |
| 9 | A_g | 4.04 | 306.95 | 0.784×10^6 | 2764 |
| 10 | A_g | 4.09 | 303.26 | 0.960×10^3 | 4 |
| 11 | A_g | 4.24 | 292.56 | 0.822×10^3 | 3 |
| 12 | A_g | 4.39 | 282.40 | 0.106×10^5 | 44 |
| 13 | A_g | 4.49 | 276.11 | 0.416×10^3 | 2 |
| 14 | A_g | 4.52 | 274.28 | 0.155×10^4 | 7 |
| 15 | A_g | 4.55 | 272.47 | 0.805×10^3 | 4 |
| 16 | A_g | 4.57 | 271.28 | 0.120×10^5 | 54 |

Table S20: Summary of CAM-B3LYP/6-31G(d,p) calculations of TPA properties for trimer (model A) *in vacuo*.

| | Symmetry | ΔE_{vert} [eV] | λ_{vert} [nm] | δ^{TPA} [au] | σ^{TPA} [GM] |
|----|----------|-------------------------------|------------------------------|----------------------------|----------------------------|
| 2 | A_g | 2.60 | 477.47 | 1.83×10^3 | 3 |
| 3 | A_g | 2.96 | 418.60 | 4.12×10^3 | 8 |
| 4 | A_g | 3.04 | 408.36 | 4.87×10^3 | 10 |
| 5 | A_g | 3.59 | 345.05 | 7.06×10^4 | 197 |
| 6 | A_g | 3.70 | 334.83 | 4.71×10^4 | 139 |
| 7 | A_g | 3.74 | 331.54 | 9.74×10^2 | 3 |
| 8 | A_g | 3.76 | 329.91 | 1.29×10^4 | 39 |
| 9 | A_g | 3.84 | 323.21 | 2.85×10^3 | 9 |
| 10 | A_g | 3.85 | 321.65 | 7.75×10^3 | 25 |
| 11 | A_g | 3.89 | 318.57 | 9.08×10^3 | 30 |
| 12 | A_g | 3.92 | 316.26 | 3.40×10^5 | 1128 |
| 13 | A_g | 3.94 | 314.10 | 3.51×10^2 | 1 |
| 14 | A_g | 3.97 | 312.14 | 9.97×10^4 | 339 |
| 15 | A_g | 4.01 | 309.14 | 1.38×10^5 | 479 |
| 16 | A_g | 4.07 | 304.94 | 6.29×10^4 | 224 |
| 17 | A_g | 4.08 | 304.02 | 2.76×10^4 | 99 |
| 18 | A_g | 4.12 | 301.23 | 1.30×10^4 | 47 |
| 19 | A_g | 4.16 | 298.12 | 1.27×10^3 | 5 |
| 20 | A_g | 4.24 | 292.16 | 2.39×10^5 | 928 |
| 21 | A_g | 4.33 | 286.11 | 5.88×10^2 | 2 |

Table S21: Unsigned transition moments along cartesian z direction between electronic states for monomer and dimer (model A). All calculations were performed at the CAM-B3LYP/6-31G(d,p) level of theory. Shown are also the diagonal components of second-order transition moment tensor (S_{ii}). Key transition moments are marked in red colour.

| MONOMER $ \langle i \hat{\mu}_z j\rangle $ | | | | | | | | | |
|---|---------|---------|---------|---------|---------|---------|---------|---------|---------|
| $S_{xx} = 44$ au., $S_{yy} = -6$ au., $S_{zz} = 1449$ au. | | | | | | | | | |
| | 1 A_g | 2 A_g | 3 A_g | 4 A_g | 5 A_g | 6 A_g | 7 A_g | 8 A_g | 9 A_g |
| 1 A_u | 3.9035 | 0.2015 | 0.3056 | 5.1256 | 0.2461 | 0.1616 | 0.2511 | 0.4076 | 0.1110 |
| 2 A_u | 0.1095 | 0.1055 | 0.0255 | 0.1886 | 0.0955 | 0.0057 | 0.0583 | 0.0729 | 0.0024 |
| 3 A_u | 0.7229 | 0.3330 | 2.7916 | 1.4063 | 0.7657 | 4.3841 | 0.0775 | 0.1356 | 1.0060 |
| 4 A_u | 3.1147 | 0.9531 | 0.9938 | 4.2807 | 1.1222 | 1.0837 | 0.4173 | 0.5619 | 0.9041 |
| 5 A_u | 0.9059 | 5.5311 | 0.1753 | 0.9886 | 4.2448 | 1.0208 | 0.5115 | 1.0782 | 1.6408 |
| 6 A_u | 0.8055 | 0.7183 | 0.3085 | 4.7109 | 1.2498 | 1.2815 | 0.3712 | 0.1682 | 0.8129 |
| 7 A_u | 0.7919 | 0.7144 | 4.4795 | 0.8310 | 1.7749 | 10.4168 | 0.2374 | 0.3450 | 0.7523 |
| 8 A_u | 0.2616 | 0.2085 | 0.1559 | 0.7023 | 0.0056 | 0.2304 | 0.0762 | 0.0284 | 0.0262 |

| DIMER $ \langle i \hat{\mu}_z j\rangle $ | | | | | | | | | |
|--|---------|---------|---------|---------|---------|---------|---------|---------|---------|
| $S_{xx} = 161$ au., $S_{yy} = 36$ au., $S_{zz} = 1780$ au. | | | | | | | | | |
| | 1 A_g | 2 A_g | 3 A_g | 4 A_g | 5 A_g | 6 A_g | 7 A_g | 8 A_g | 9 A_g |
| 1 A_u | 4.5883 | 0.1298 | 0.7378 | 0.3339 | 0.1472 | 0.2981 | 0.2409 | 0.6507 | 4.3783 |
| 2 A_u | 2.7810 | 0.5008 | 1.3140 | 0.0175 | 0.0814 | 0.0996 | 0.0074 | 0.0314 | 0.8110 |
| 3 A_u | 0.0717 | 0.0678 | 0.0265 | 0.5385 | 0.8002 | 0.6438 | 0.0279 | 0.4220 | 0.3346 |
| 4 A_u | 0.2202 | 0.1168 | 0.0831 | 0.1273 | 0.1417 | 0.0545 | 0.0271 | 0.1791 | 0.3152 |
| 5 A_u | 0.3219 | 0.2038 | 0.0819 | 0.0538 | 0.1997 | 0.1964 | 3.0003 | 0.2294 | 0.2610 |
| 6 A_u | 3.2816 | 0.4887 | 0.0860 | 0.1480 | 0.1837 | 0.8187 | 0.0327 | 1.0181 | 3.7771 |
| 7 A_u | 1.6193 | 0.0400 | 0.1386 | 0.2095 | 0.6029 | 1.2435 | 0.2287 | 2.6266 | 1.1415 |
| 8 A_u | 0.4602 | 4.9968 | 0.0520 | 2.1055 | 2.8189 | 0.2197 | 0.1619 | 0.5511 | 0.1927 |

Table S22: One-photon absorption spectra of dimer (model B) *in vacuo* determined at the CAM-B3LYP/6-31G(d,p) level of theory.

| | Symmetry | ΔE_{vert} [eV] | λ_{vert} [nm] | f | orb. transitions |
|----|----------|-------------------------------|------------------------------|--------|------------------------------|
| 2 | A_g | 2.7456 | 451.57 | 0.0000 | HOMO-1→LUMO, HOMO→LUMO+1 |
| 1 | A_u | 2.7521 | 450.51 | 1.2382 | HOMO→LUMO |
| 3 | A_g | 3.2998 | 375.74 | 0.0000 | HOMO-1→LUMO, HOMO→LUMO+1 |
| 2 | A_u | 3.4339 | 361.05 | 0.6748 | HOMO-1→LUMO+1 |
| 3 | A_u | 3.7772 | 328.25 | 0.0086 | HOMO-10→LUMO, HOMO→LUMO+10 |
| 4 | A_u | 3.7958 | 326.64 | 0.0154 | HOMO-3→LUMO |
| 4 | A_g | 3.8016 | 326.13 | 0.0000 | HOMO-11→LUMO, HOMO→LUMO+11 |
| 5 | A_g | 3.8638 | 320.89 | 0.0000 | HOMO→LUMO+3 |
| 5 | A_u | 3.9162 | 316.60 | 0.1927 | HOMO-1→LUMO+3 |
| 6 | A_g | 3.9169 | 316.53 | 0.0000 | HOMO-1→LUMO+2 |
| 6 | A_u | 3.9668 | 312.55 | 0.2354 | HOMO-3→LUMO, HOMO→LUMO+2 |
| 7 | A_g | 3.9975 | 310.15 | 0.0000 | HOMO-2→LUMO |
| 7 | A_u | 4.0688 | 304.72 | 0.4313 | HOMO→LUMO+4 |
| 8 | A_g | 4.0872 | 303.35 | 0.0000 | HOMO-2→LUMO |
| 8 | A_u | 4.1385 | 299.58 | 0.2815 | HOMO-4→LUMO |
| 9 | A_g | 4.1687 | 297.41 | 0.0000 | HOMO-5→LUMO, HOMO→LUMO+9 |
| 10 | A_g | 4.1829 | 296.41 | 0.0000 | HOMO→LUMO+5 |
| 9 | A_u | 4.2017 | 295.08 | 0.0150 | HOMO-1→LUMO+5, HOMO→LUMO+8 |
| 10 | A_u | 4.3286 | 286.43 | 0.0238 | HOMO-7→LUMO+2, HOMO-6→LUMO+3 |
| 11 | A_g | 4.3336 | 286.10 | 0.0000 | HOMO-7→LUMO+3, HOMO-6→LUMO+2 |

Table S23: One-photon absorption spectra of trimer (model B) *in vacuo* determined at CAM-B3LYP/6-31G(d,p) level of theory.

| | Symmetry | ΔE_{vert} [eV] | λ_{vert} [nm] | f |
|----|----------|-------------------------------|------------------------------|--------|
| 1 | A_u | 2.7907 | 444.28 | 0.0165 |
| 2 | A_g | 2.8116 | 440.98 | 0.0000 |
| 2 | A_u | 2.8605 | 433.43 | 1.5040 |
| 3 | A_u | 3.3054 | 375.10 | 0.0375 |
| 3 | A_g | 3.3070 | 374.91 | 0.0000 |
| 4 | A_g | 3.3793 | 366.90 | 0.0000 |
| 4 | A_u | 3.4191 | 362.63 | 0.7109 |
| 5 | A_u | 3.7592 | 329.81 | 0.0073 |
| 5 | A_g | 3.8011 | 326.18 | 0.0000 |
| 6 | A_u | 3.8052 | 325.83 | 0.0002 |
| 6 | A_g | 3.8377 | 323.07 | 0.0000 |
| 7 | A_u | 3.8851 | 319.13 | 0.0260 |
| 8 | A_u | 3.9307 | 315.43 | 0.0237 |
| 7 | A_g | 3.9496 | 313.91 | 0.0000 |
| 8 | A_g | 3.9904 | 310.71 | 0.0000 |
| 9 | A_u | 3.9962 | 310.26 | 0.4888 |
| 9 | A_g | 4.0515 | 306.02 | 0.0000 |
| 10 | A_u | 4.0613 | 305.28 | 0.0301 |
| 10 | A_g | 4.0856 | 303.47 | 0.0000 |
| 11 | A_u | 4.0957 | 302.72 | 0.0030 |

Table S24: Summary of CAM-B3LYP/6-31G(d,p) calculations of TPA properties for dimer (model B) *in vacuo*.

| | Symmetry | ΔE_{vert} [eV] | λ_{vert} [nm] | δ^{TPA} [au] | σ^{TPA} [GM] |
|----|----------|-------------------------------|------------------------------|----------------------------|----------------------------|
| 2 | A_g | 2.75 | 451.57 | 4.13×10^2 | 1 |
| 3 | A_g | 3.30 | 375.74 | 3.41×10^3 | 8 |
| 4 | A_g | 3.80 | 326.13 | 2.63×10^2 | 1 |
| 5 | A_g | 3.86 | 320.89 | 3.47×10^3 | 11 |
| 6 | A_g | 3.92 | 316.53 | 1.04×10^4 | 35 |
| 7 | A_g | 4.00 | 310.15 | 1.13×10^5 | 391 |
| 8 | A_g | 4.09 | 303.35 | 1.59×10^5 | 575 |
| 9 | A_g | 4.17 | 297.41 | 6.37×10^3 | 24 |
| 10 | A_g | 4.18 | 296.41 | 2.49×10^5 | 940 |
| 11 | A_g | 4.33 | 286.10 | 3.06×10^3 | 12 |
| 12 | A_g | 4.48 | 276.76 | 7.23×10^2 | 3 |
| 13 | A_g | 4.55 | 272.69 | 3.67×10^3 | 16 |
| 14 | A_g | 4.59 | 270.26 | 9.19×10^2 | 4 |
| 15 | A_g | 4.62 | 268.32 | 3.64×10^3 | 17 |
| 16 | A_g | 4.67 | 265.27 | 8.10×10^2 | 4 |

Table S25: Summary of CAM-B3LYP/6-31G(d,p) calculations of TPA properties for trimer (model B) *in vacuo*.

| | Symmetry | ΔE_{vert} [eV] | λ_{vert} [nm] | δ^{TPA} [au] | σ^{TPA} [GM] |
|----|----------|-------------------------------|------------------------------|----------------------------|----------------------------|
| 2 | A_g | 2.81 | 440.98 | 1.20×10^2 | < 1 |
| 3 | A_g | 3.31 | 374.91 | 5.21×10^3 | 12 |
| 4 | A_g | 3.38 | 366.90 | 4.80×10^2 | 1 |
| 5 | A_g | 3.80 | 326.18 | 2.87×10^2 | 1 |
| 6 | A_g | 3.84 | 323.07 | 1.44×10^3 | 5 |
| 7 | A_g | 3.95 | 313.91 | 1.46×10^4 | 49 |
| 8 | A_g | 3.99 | 310.71 | 5.20×10^4 | 179 |
| 9 | A_g | 4.05 | 306.02 | 2.63×10^4 | 93 |
| 10 | A_g | 4.09 | 303.47 | 1.42×10^4 | 51 |
| 11 | A_g | 4.11 | 301.87 | 7.93×10^4 | 289 |
| 12 | A_g | 4.14 | 299.51 | 5.78×10^4 | 214 |
| 13 | A_g | 4.21 | 294.84 | 4.20×10^3 | 16 |
| 14 | A_g | 4.24 | 292.79 | 9.26×10^2 | 4 |
| 15 | A_g | 4.30 | 288.65 | 1.79×10^5 | 715 |
| 16 | A_g | 4.40 | 281.62 | 1.99×10^4 | 83 |
| 17 | A_g | 4.44 | 279.29 | 2.82×10^3 | 12 |
| 18 | A_g | 4.48 | 276.44 | 1.57×10^2 | 1 |
| 19 | A_g | 4.50 | 275.56 | 8.42×10^2 | 4 |
| 20 | A_g | 4.53 | 273.75 | 1.12×10^3 | 5 |
| 21 | A_g | 4.58 | 270.43 | 1.80×10^3 | 8 |

References

1. M. G. Humphrey, B. Babgi, L. Rigamonti, M.P. Cifuentes, T.C. Corkery, M.D. Randles, T. Schwich, S. Petrie, R. Stranger, A. Teshome, I. Asselberghs, K. Clays, M. Samoc, *J. Am. Chem. Soc.* 2009, **131**, 10293-10307
2. M. Sheik-Bahae, A. A. Said, T. H. Wei, D. J. Hagan and E. W. Van Stryland, *IEEE J. of Quant. Elec.*, 1990, **26**, 760-769.
3. L. Y. Bu, Y. P. Li, J. F. Wang, M. X. Sun, M. Zheng, W. Liu, S. F. Xue and W. J. Yang, *Dyes Pigments*, 2013, **99**, 833-838.
4. X. Q. Zhang, Z. G. Chi, J. Y. Zhang, H. Y. Li, B. J. Xu, X. F. Li, S. W. Liu, Y. Zhang and J. R. Xu, *J. Phys. Chem. B*, 2011, **115**, 7606-7611.
5. X. Q. Zhang, Z. G. Chi, H. Y. Li, B. J. Xu, X. F. Li, W. Zhou, S. W. Liu, Y. Zhang and J. R. Xu, *Chem-Asian J*, 2011, **6**, 808-811.
6. G. G. Shan, H. B. Li, D. X. Zhu, Z. M. Su and Y. Liao, *J. Mater. Chem.*, 2012, **22**, 12736-12744.
7. M. J. Frisch, G. W. Trucks, H. B. Schlegel, G. E. Scuseria, M. A. Robb, J. R. Cheeseman, G. Scalmani, V. Barone, B. Mennucci, G. A. Petersson, H. Nakatsuji, M. Caricato, X. Li, H. P. Hratchian, A. F. Izmaylov, J. Bloino, G. Zheng, J. L. Sonnenberg, M. Hada, M. Ehara, K. Toyota, R. Fukuda, J. Hasegawa, M. Ishida, T. Nakajima, Y. Honda, O. Kitao, H. Nakai, T. Vreven, J. A. Montgomery, Jr., J. E. Peralta, F. Ogliaro, M. Bearpark, J. J. Heyd, E. Brothers, K. N. Kudin, V. N. Staroverov, R. Kobayashi, J. Normand, K. Raghavachari, A. Rendell, J. C. Burant, S. S. Iyengar, J. Tomasi, M. Cossi, N. Rega, J. M. Millam, M. Klene, J. E. Knox, J. B. Cross, V. Bakken, C. Adamo, J. Jaramillo, R. Gomperts, R. E. Stratmann, O. Yazyev, A. J. Austin, R. Cammi, C. Pomelli, J. W. Ochterski, R. L. Martin, K. Morokuma, V. G. Zakrzewski, G. A. Voth, P. Salvador, J. J. Dannenberg, S. Dapprich, A. D. Daniels, Ö. Farkas, J. B. Foresman, J. V. Ortiz, J. Cioslowski, and D. J. Fox, Gaussian 09, Revision **E.01**, Gaussian, Inc., Wallingford CT, 2009.
8. K. Aidas, C. Angeli, K. L. Bak, V. Bakken, R. Bast, L. Boman, O. Christiansen, R. Cimiraglia, S. Coriani, P. Dahle, E. K. Dalskov, U. Ekström, T. Enevoldsen, J. J. Eriksen, P. Ettenhuber, B. Fernández, L. Ferrighi, H. Fliegl, L. Frediani, K. Hald, A. Halkier, C. Hättig, H. Heiberg, T. Helgaker, A. C. Hennum, H. Hettema, E. Hjertenæs, S. Høst, I.-M. Høyvik, M. F. Iozzi, B. Jansik, H. J. Aa. Jensen, D. Jonsson, P. Jørgensen, J. Kauczor, S. Kirpekar, T. Kjærgaard, W. Klopper, S. Knecht, R. Kobayashi, H. Koch, J. Kongsted, A. Krapp, K. Kristensen, A. Ligabue, O. B. Lutnæs, J. I. Melo, K. V. Mikkelsen, R. H. Myhre, C. Neiss, C. B. Nielsen, P. Norman, J. Olsen, J. M. H. Olsen, A. Osted, M. J. Packer, F. Pawłowski, T. B. Pedersen, P. F. Provasi, S. Reine, Z. Rinkevicius, T. A. Ruden, K. Ruud, V. Rybkin, P. Salek, C. C. M. Samson, A. Sánchez de Merás, T. Saue, S. P. A. Sauer, B. Schimmelpfennig, K. Sneskov, A. H. Steindal, K. O. Sylvester-Hvid, P. R. Taylor, A. M. Teale, E. I. Tellgren, D. P. Tew, A. J. Thorvaldsen, L. Thøgersen, O. Vahtras, M. A. Watson, D. J. D. Wilson, M. Ziolkowski, and H. Ågren, "The Dalton quantum chemistry program system", *WIREs Comput. Mol. Sci.* 2014, **4**, 269–284.
9. a) Y. Ren, J. W. Y. Lam, Y. Dong, B. Z. Tang, K. S. Wong, *J. Phys. Chem. B* 2005, 109, 1135-1140; b) G. Mu, W. Zhang, P. Xu, H. Wang, Y. Wang, L. Wang, S. Zhuang, X. Zhu, *J. Phys. Chem. C* 2014, 118, 8610-8616.